submitted to Progress in Photovoltaics: Research and Applications

Degradation in Photovoltaic Encapsulant Transmittance: Results of the First PVQAT TG5 Artificial Weathering Study

David C. Miller,[1] Jayesh G. Bokria,[2] David M. Burns,[3] Sean Fowler,[4] Xiaohong Gu,[5] Peter L. Hacke,[1] Christian C. Honeker,[6] Michael D. Kempe,[1] Michael Köhl,[7] Nancy H. Phillips,[8] Kurt P. Scott,[9] Ashish Singh,[10] Shigeo Suga,[11] Shin Watanabe,[11] and Allen F. Zielnik[8]

[1]National Renewable Energy Laboratory (NREL), 15013 Denver West Parkway, Golden, CO 80401, USA
[2]Specialized Technology Resources, Inc. (STR), 10 Water Street, Enfield, CT, USA 06082
[3]The 3M Company, 3M Center, Building 235-67-15, St. Paul, MN, 55144, USA
[4]Q-Lab Corporation, 800 Canterbury Road, Cleveland, OH 44145 USA
[5]National Institute of Standards and Technology (NIST), 100 Bureau Dr., Gaithersburg, MD 20899-8615, USA
[6]Fraunhofer Center for Sustainable Energy Systems (CSE), 5 Channel Center, Boston, MA 02210, USA
[7]Fraunhofer Institute for Solar Energy Systems (ISE), Heidenhofstrasse 2, 79110 Freiburg, Germany
[8]DuPont Photovoltaic Solutions, Wilmington, DE, 19803 USA
[9]Atlas Material Testing Technology L.L.C., 1500 Bishop Court, Mount Prospect, IL 60056, USA
[10]RenewSys India Pvt Ltd., Bommasandra – Jigani Link Road Industrial Area, Bangalore – 560 105, India
[11]Suga Test Instruments Co., Ltd., 5-4-14 Shinjuku, Shinjuku-ku, 160-0022, Tokyo Japan

**Corresponding author*: David.Miller@nrel.gov +1 3033847855 http://www.nrel.gov/pv/performance_reliability/

ABSTRACT

Reduced optical transmittance of encapsulants resulting from ultraviolet (UV) degradation is frequently identified as a cause of decreased performance through the service life of photovoltaic modules. However, the present module safety and qualification standards apply short UV doses, only capable of examining design robustness and "infant mortality" failures. Furthermore, essential information remains unknown that might be used to screen encapsulants through product lifetime. We conducted an interlaboratory study to provide the understanding that will be used toward developing a higher-fidelity, more-rigorous UV weathering test. Five representative known formulations of poly(ethylene-co-vinyl acetate) were studied, in addition to one thermoplastic polyurethane material. Replicate laminated silica/polymer/silica specimens were examined at seven institutions using a variety of indoor chambers (including xenon, UVA-340, and metal-halide light sources). Specimens were artificially weathered for 180 cumulative days at steady-state accelerated test conditions, predesignated relative to the default irradiance of 1.0 $W \cdot m^{-2} \cdot nm^{-1}$ at 340 nm, chamber temperature of 60°C, and chamber relative humidity of 30%. The solar-weighted transmittance, yellowness index, and the UV cut-off wavelength—each determined from the measured hemispherical transmittance—are examined to provide understanding and guidance for the UV light source (type lamp and filters), temperature, and humidity used in accelerated UV aging tests. The relative efficacy of xenon-arc and UVA-340 fluorescent sources and the typical range of activation energy for degradation is quantified from the experiments.

KEYWORDS: durability, EVA, reliability, thermal activation, TPU

1. INTRODUCTION

The discoloration of encapsulants resulting from ultraviolet radiation (UV) degradation is a known degradation mode for photovoltaic (PV) modules, where vulnerable encapsulant formulations exhibit measurable loss in performance through the module lifetime [1]. As summarized in Table I, existing protocols examining the general robustness of PV modules include the IEC 61730 (safety) [2] and IEC 61215 (design qualification and type approval) [3] standards. Details in the table include: the standard and its version (year); the test within the standard, and its associated index; the type of irradiance source; the type of UV filter; the broadband UV irradiance (from 280 nm to 400 nm); the tolerance for UV uniformity and the associated waveband ranges; the spectral distribution of UV radiation and the associated waveband range; the cumulative radiant exposure for the test; the specimen temperature; and the specimen relative humidity. UVA-340 fluorescent and metal-halide lamps are not specified but are typically used in the industry for the tests in Table I. Other than the minimum wavelength of 280 nm and the uniformity of the flux, the requirements for a UV source spectrum are not sufficiently established to specify the appropriate lamps and filters. In IEC 61215-2, UV Preconditioning is, however, specified to be monitored from 280 nm to 400 nm with 3% to 10% of the applied radiation occurring from 280 nm to 320 nm. In contrast, ASTM D7869 [5] specifies the source spectrum over 13 wavebands to achieve higher fidelity to the terrestrial solar spectrum. IEC 61215-2 specifies a UV Preconditioning of 54 $MJ \cdot m^{-2}$ (i.e., 15 $kWh \cdot m^{-2}$), which could be encountered in as little as forty 8-hour-UV-days of field exposure to the AM1.5G total UV spectrum [4]. IEC 61730-2 presently prescribes up to 4x the UV exposure in IEC 61215-2, which is also much less than expected through module field life. Establishing module reliability for long-term use, e.g., comparable to the desired lifetime of 25 years. While the specimen temperature is specified (60 °C), the specimen relative humidity is not specified for the tests. Relative to that, the coupling between relevant stress factors (i.e., UV, temperature, and humidity) is not well established such that they might be prescribed for artificial weathering or that appropriate locations might be chosen for comparative natural weathering. Lastly, the activation energy for the UV degradation of PV encapsulants has not been established to provide a technical basis for prescribing and interpreting artificial tests.

We conducted a set of experiments to provide the understanding that will be used to develop exposures as part of a weathering test method for transparent PV packaging materials, including encapsulants. The study was conducted on laminated coupon specimens, with the goal of developing a relatively inexpensive, high-fidelity

weathering test. Because no single institution had all of the resources to run the numerous exposure conditions, seven institutions collaborated in this work, as represented by the authors of this paper.

The goals of the encapsulant transmittance study include the following:

- Investigate the spectral requirements for different light sources by comparing aged specimens, e.g., Xe-arc and UVA-340 (type 1A) fluorescent lamps. The inclusion of visible light was considered in addition to UV radiation.
- Determine if there is significant coupling between relevant stress factors, i.e., UV, temperature, and moisture (relative humidity, %RH). The study sought to identify what factors need to be considered in an accelerated test for evaluating degradation of optical performance of polymeric encapsulants.
- Quantify the activation energy, E_a, for the degradation of transmittance. This includes providing a sense of the range of the E_a values that may be present in encapsulants by examining "known bad," "known good," and "intermediate" material formulations.

2. BACKGROUND

The degradation of encapsulants used for PV modules subject to UV weathering has been examined previously [6,7,8]—particularly after the incident at the Carrizo Plains concentrator installation using the EVA PHOTOCAP A9918P [9], [10]. The weathering of poly(ethylene-co-vinyl acetate) (EVA) is summarized in detail in Ref. [11], including formulations (as well as unformulated EVA) and light sources not always considered suitable to the PV application. Artificial or natural weathering can increase molecular cross-linking (gel content), reduce transmittance (with visual discoloration), decrease elastic modulus and reduce tensile strength, and form acetic acid. In many studies, photooxidative bleaching of the chromophore species (or the prevention of chromophore formation) was observed to occur for EVA located 1) at the edges of cells or coupons, 2) where no cell is present, and 3) at cracks in cells.

The former studies, e.g., [6], highlight the reduction in transmittance and the effect on characteristics including gel content as well as the chemical byproducts of EVA. Regarding the mechanism enabling degradation, early work suggested the formation of long chains of conjugated unsaturated sequences (polyenes), generated by the photo-induced deacetylation of vinyl acetate[12],[13]. Other studies focused on α- and β-unsaturated structures present in the EVA resin that were speculated to contribute to UV degradation and discoloration [],[].

More recent studies, e.g., [7],[8], instead identify that the degradation of EVA results from interactions between stabilization additives. The most recent studies also examine interactions between pairs or more complex combinations of additives [16] or highlight the interactions between additives (such as peroxide, remaining after curing) and other components in PV modules [17]. The early results of the study here [18] suggested that the additives play a crucial role in EVA discoloration, e.g., no reduction in transmittance was observed for an EVA formulation where no UV absorber was present.

Concepts critical to this study include the source spectrum, optical throughput of the encapsulant and packaging components, action and activation spectrum, and the law of reciprocity. The spectral distribution for common UV sources—including UVB-313 (type 2) fluorescent, UVA-340 fluorescent, xenon arc, and metal-halide lamps—are compared to the terrestrial solar spectrum in Ref. [11]. The spectral bandwidth and fidelity of artificial sources depends on the type of lamp as well as the filters used. The optical transmittance and absorptance of common PV encapsulants and packaging materials (e.g., glass) is described in Ref. [19]. The action spectrum refers to the wavelength sensitivity of a particular material characteristic, such as transmittance. The activation spectrum is the convolution of the source spectrum and the action spectrum. The law of reciprocity refers to the correlation between the degradation, intensity, and duration of UV exposure [11,20,21,22], e.g., Schwarzchild's law, Equation 1. In the equation, H represents the radiant exposure (taken as a proxy for the degradation) $\{J \cdot m^{-2}\}$, E the irradiance $\{W \cdot m^{-2}\}$; and t, the time {s}.

$$H = Et^p \quad (1)$$

3. EXPERIMENTAL

A set of encapsulant formulations was weathered as glass/encapsulant/glass coupons under a variety of different steady-state conditions. As summarized in Table II, six different encapsulation materials were examined in the transmittance study. The formulation additives (including their purpose, make, and concentration) are identified in Table II [18] for the EVA samples. "N/A" is used to indicate where an additive was not used, and "?" indicates where the presence or composition of an additive is not known. The material designation used in the figures and text is indicated at the bottom of the table. The specimens include: those prone to discoloration ("known bad"); a subsequent generation of EVA product ("improved"); a formulation expected to change minimally ("known good"); and a representative contemporary material ("modern"). Two of

the formulations are frequently examined in the PV literature ("slow cure" and "fast cure"). The five formulations of EVA were fabricated at Specialized Technology Resources, Inc. (STR). One thermoplastic polyurethane (TPU) product from outside the PV industry, known to discolor rapidly from natural weathering, was also examined. It should be mentioned that Elvax PV 1400 resin contains ~550 ppm of butylated hydroxytoluene (BHT), which serves as an anti-oxidant and heat stabilizer during its processing.

To quantify the glass- and phase transition-temperatures for the encapsulants relative to artificial weathering temperatures applied in this study, differential scanning calorimetry (DSC) was performed with a Q2000 instrument (TA Instruments, Inc). The 2-Hz data were taken from the second of two consecutive cycles (from $-100 \leq T \leq 250$°C) at the rate of 10^0C·min^{-1} in a nitrogen environment (50 mL·min^{-1} purge). Measurements were performed in a non-hermetic aluminum crucible. Specimens were stamped to size using a 4.8 mm diameter punch, resulting in a specimen mass on the order of 7 mg. Melt- or crystallization-transitions were assessed from the local-maxima or -minima using the linear peak integration algorithm, whereas glass transitions were assessed within the transition region using the glass transition algorithm in the Universal Analysis software.

Weathering specimens were made by first laminating a 36.8-cm × 36.8-cm silica/encapsulant/silica stack using a thickness-specific removable layer to ensure good (0.45±0.03 mm) thickness uniformity. Lamination was performed for 8 min at 145°C using a commercial laminator (Model LM-404, AstroPower Inc.). The resulting samples were then diced into 5.1-cm × 5.1-cm coupons using an abrasive water-jet saw. Diced specimens were then preconditioned in temperature/humidity chambers for 1 month to achieve a baseline moisture concentration in the polymer similar to that applied in artificial weathering. When not being examined at readpoints, specimens were stored in damp chambers to maintain their internal concentration of water. Silica glass (transmitting above 202 nm) was used rather than industry-standard soda-lime glass (transmitting above 295 nm), so that the glass would not attenuate UV radiation.

The weathering conditions used in the experiments are summarized in Table III, including: the lamp type (i.e., xenon arc, hydrargyrum quartz iodide "HQI" metal-halide, or UVA-340 fluorescent bulb); the optical filters (i.e., daylight fulfilling ASTM D7869 ["D7869 compliant"], daylight not fulfilling ASTM D7869 ["Daylight"], quartz glass, and type S borosilicate glass ["s-boro"]); the irradiance at the specimen plane (in W·m^{-2}·nm^{-1}, indicated at 340 nm); the chamber temperature setting (ChT); and the chamber relative humidity setting (ChRH).

Participant 4 performed experiments with no irradiation ("N/A"). Combinations of filters are indicated with the inner filter (adjacent to the source) then the outer filter (exposed to the chamber air). The study was originally designed for the nominal settings of 1.0 $W \cdot m^{-2} \cdot nm^{-1}$ at 340 nm, with the indoor chamber temperature setpoint of 60°C, and the chamber controlled to 30% RH. Alternate conditions were sometimes applied for specific purposes including: ChT of 45°, 60°, or 80°C for an Arrhenius analysis; ChRH of 50% to study the effect of moisture; or ChT/ChRH combinations of 80°C/20% and 90°C/20%, which were proposed during the development of the IEC TS 62788-7-2 UV weathering standard [23]. Other experiments were conducted based on the control available for commercial weathering equipment, e.g., ChRH of ~7%, indicating the uncontrolled approximate %RH of the chamber at the specified ChT. The chamber black-panel temperature was not specified to be controlled during the study. Cumulative radiant exposure is reported in Figure 3, Figure 4,Figure 5, Figure 6, Figure 14, Figure 15 for the wavelength range 295 nm ≤ λ ≤ 360 nm so that the results may be readily compared between Xe and UVA-340 sources, as suggested in Ref. [24].

Representative spectra for the irradiation sources used in the study are shown in Figure 1. The spectra include a xenon lamp (shown for ASTM D7869 compliant/quartz as well as the type S-borosilicate/quartz glass filter combinations), a UVA-340 fluorescent lamp [25], an HQI metal-halide lamp, and the AM1.5 global spectrum [26]. Spectra for artificial sources were obtained from participating laboratories or equipment vendors and were not independently verified. The change in source spectra with the lamp age is not considered in Figure 1. All spectra have been normalized to E = 1.0 $W \cdot m^{-2} \cdot nm^{-1}$ at 340 nm so that the spectral content may be compared, and the information to compare the absolute magnitude of the irradiance is shown in Table III. A specific make of UVA-340 lamp was used by participant 3 in Table III, not pictured, which featured additional radiation above 400 nm, consisting of a ~120-nm-wide peak, centered at 560 nm. Importantly, the spectra in Figure 1 do not account for the angular incidence at the specimen plane; in practice, the angle of acceptance for the optics used to facilitate closed-loop control in commercial weathering chambers is typically on the order of 45 degrees, i.e., intermediate to the angular distribution of AM1.5 direct spectrum and the AM1.5 global spectrum. The AM1.5 global spectrum is used for reference in this study because it more closely resembles the optical response of a PV module (where Fresnel reflection at an air/glass interface begins to become significant at about 60 degrees [27]).

As summarized in Table III, optical transmittance was measured using a variety of spectrophotometers equipped with integrating spheres. The table identifies the make, model, and measurement range for the instruments used in the experiment. Transmittance measurements were obtained at the nominal cumulative exposure of 0, 15, 30, 45, 60, 75, 90, 120, and 180 days. All participants obtained transmittance measurements at the center of the specimens. Additional measurements were performed at the specimen periphery (within ~0.5 cm of the edge) at the laboratories of participants 2, 5, and 6. Participant 3 used two spectrophotometers to achieve the combined measurement range of 320–2,400 nm. The study intended to have measurements performed according to the procedure in IEC 62788-1-4 [28], with the 1-nm incremented measurement starting at 200 nm to quantify the critical changes from weathering in the UV wavelengths. Transmittance spectra were analyzed to provide: the representative solar-weighted transmittance of photon irradiance, τ_{rsw} [29], directly related to PV performance; the solar-weighted transmittance of photon irradiance, τ_{sw} [29], evaluated to include the broad range of the terrestrial sun; yellowness index (YI), a mathematical treatment of the spectral data that quantifies the change in color perceived by a human observer; and the UV cut-off wavelength, λ_{cUV}, which quantifies when the material becomes transmitting. YI is a more acute indicator than the characteristic of τ_{rsw}, with the threshold for interlaboratory repeatability of 0.27% rather than 0.63% [29]. The transmittance results, including spectra, are presented here for the average of measurements for three replicate specimens with the corresponding error bounds for one standard deviation (S.D.).

The reflectance of the coupon specimens was not measured in this study. Additional variation for reflectance may follow from: the use of a calibrated reflectance standard; a signal to noise ratio lesser than that of transmittance; the evolution of the crystalline content of the encapsulant with weathering; and optical interaction with chromophore species. An approximate conversion between transmittance and absorptance might, however, be obtained if the reflectance (e.g., Figure 7) is assumed not to vary with weathering (absorptance, reflectance, and transmittance must sum to 100% at all wavelengths).

Specimen temperature was verified at the participating laboratories using additional coupons. Most critical to this experiment, silica/EVA/silica coupons were used that contained a T-type thermocouple embedded in the EVA layer. A 30 American wire-gauge thermocouple (5SRTC-TT-T-30-12, Omega Engineering, Inc.) was used to minimize radiative heat transfer from the light source, to achieve a temperature close to that of the test

specimens. The coupons for temperature verification were circulated in series to each of the participants to quantify a representative specimen temperature for each experiment.

The optical absorptance of the additives in Table II was obtained using a Cary 500 dual-beam ultraviolet–visible–near-infrared (UV-VIS-NIR) spectrophotometer (Agilent Technologies Inc.) with no integrating sphere. Samples of each additive were obtained from the manufacturer and dissolved to ~0.01% wt. concentration in hexane. Additive solutions were examined in a 1-cm quartz cuvette.

Specimen photographs were obtained using a camera (40D, Canon Inc.) or SMZ-1500 Zoom Stereo microscope (Nikon Instruments Inc.) equipped with a DS-Fi1 camera (Nikon Instruments Inc.). Images were also obtained using a UVGL25 Compact Split Tube UV Lamp (UVP, LLC.), which operates at 254 and 365 nm. The UV lamp can be used to qualitatively assess the presence of formulation additives and to visualize the area of UV damage.

UV-VIS fluorescence spectroscopy [30] was performed with a FL-112XI Fluorolog-II (SPEX Industries Inc). As described in Ref. [31], the instrument uses a Xe-arc lamp source (450-W bulb), Hamamatsu R928 photomultiplier tube (PMT) emission detector, and Hamamatsu R508 PMT reference detector (with Rhodamine B as the quantum counter). Initial emission spectra were obtained using the excitation wavelength (λ_m) of 280 nm, with the response being measured from 290 to 550 nm in 1-nm increments. Initial excitation spectra were obtained using the excitation wavelengths from 280 to 540 nm in 1-nm increments, with the response being measured at 550 nm (λ_x). Subsequent emission and excitation spectra were obtained iteratively to correlate observed peaks, depending on the results of the initial scans.

4. ANALYTICAL

A degradation rate comparison (the linear application of a logarithmic “shift factor” analysis [32,33]) was sometimes applied to quantify the effects of different weathering conditions. The ratio of the slopes for different artificial weathering experiments provides a means to compare degradation between the test conditions and materials. The relative degradation rate, k_H, follows as the ratio of the slopes of the linear fit, i.e., the multiplier that is required to scale data to be parallel. The change in transmittance or YI was typically examined relative to the unaged condition. A linear fit, typically fixed to the origin, was applied in the slope analysis. The transmittance

or YI sometimes showed a change in slope with cumulative radiant exposure. For the weathering data with an inflection, only the initial data points before the perceived inflection were analyzed.

Temperature trends were analyzed using an Arrhenius fit [34]. The characteristic slope (change in transmittance or YI with respect to the change in cumulative radiant exposure) was evaluated for the experiments performed at participant 1's laboratory at the nominal ChT of 45°C, 60°C, or 80°C. The slope values were then evaluated at the verified specimen temperatures (for the coupon with an embedded thermocouple) of 47.7°C, 63.5°C, or 84.2°C, respectively, to give the activation energy. The Arrhenius analysis here does not account for the change in specimen temperature that might occur from increased optical absorptance with discoloration. The increase in specimen temperature with age is expected to be limited here because the analysis was applied up to inflections, i.e., changes in transmittance ≤2%. The uncertainty of the Arrhenius analysis was determined from the method of propagation of uncertainty. Uncertainty was first determined for the variability of transmittance or YI with respect to the variability of radiant exposure, and then, for the variation of the slope ($\Delta\tau/\Delta H$ or $\Delta YI/\Delta H$) with respect to the variation in temperature.

5. RESULTS

5.1 OPTICAL EFFECTS OF THE FORMULATION ADDITIVES

The optical absorptance of the additives used in this study is summarized in Figure 2. The UV absorbers (Cyasorb UV-531 and Tinuvin 329) both feature two absorptance peaks. In Figure 2, these additives provide UV absorption between 280 nm and 380 nm. The hindered amine light stabilizers (Tinuvin 770 and Tinuvin 123) and anti-oxidants (Naugard P and BHT) instead show strong absorptance for λ <240 nm. The curing agents (Lupersol 101 and TBEC) are not shown in Figure 2 because they are expected to decompose during the lamination and subsequent life of a PV module.

The characterization in Figure 2 importantly identifies the UV absorbers in Table II that are the primary additives absorbing UV radiation from ~280–380 nm. In comparison, the other additives in Table II are practically transparent above ~290 nm. The optical response (bandwidth and magnitude) of the additives in Figure 2 will be affected by their concentration. Interaction between additives may also affect the optical response, e.g., the exact wavelength of greatest absorptance.

5.2 GLASS- AND PHASE TRANSITION-TEMPERATURES

The phase-transition temperatures are summarized in Table IV, which includes glass-transition temperature (T_g or T_α), melt-transition temperature (T_m), and crystallization-transition temperature (T_c). T_g is provided in the table for the average of the final heating and cooling ramps during the DSC measurement. The average T_g for all the EVA materials in this study is -32.3 °C. A hysteresis is observed between T_m (56.4 °C on average) and T_c (36.6 °C) for the EVAs in this study. T_g for TPU is similar to EVA, but T_m and T_c are greater for TPU. Comparing Table IV to Table III, the T_m and T_c for the EVAs and TPU overlap with the ChT used in experiments in this study, while T_g always occurs at a lower temperature than any ChT applied in the study.

5.3 REPRESENTATIVE TRANSMITTANCE AND YELLOWNESS INDEX RESULTS

The evolution of τ_{rsw} is shown in Figure 3 for the applied conditions of E_{340} of 1.0 $W \cdot m^{-2} \cdot nm^{-1}$, ChT of 60°C, and ChRH of 50%. Cumulative radiant exposure is indicated in Figure 3 for the wavelength range 295 nm $\leq \lambda \leq$ 360 nm. The transmittance with age is *decreased* by the end of the experiment by 5.2% and 2.3% for TPU and EVA-A, respectively, but is *increased* by as much as 0.8% for EVA-C during the experiment. τ_{rsw} changed by <0.6% for EVA-B, EVA-D, and EVA-E through the experiment.

The discoloration with age for the materials weathered by participant 5 is compared in Figure 4. Some of the materials show a sustained increase in YI over the course of weathering, whereas other materials show a discrete inflection in the data. To distinguish the materials with an inflection in the figure, their label is located at the inflection with an arrow, and the subsequent data are connected with a dashed line. Inflections were not always obvious in the τ_{rsw} data (e.g., compare EVA-D in Figure 3) relative to the YI data.

Figure 3 and Figure 4 provide representative examples, but the specific trends for transmittance and yellowness sometimes varied between the different materials and different experiments in the study. The following formulation-specific observations apply for the study:

- TPU demonstrated the greatest loss in τ_{rsw} with a corresponding increase in YI in 12/16 experiments. (None of the materials showed a definite change in τ_{rsw} or YI in the experiments at participant 4 at 40°C and 60°C, where no irradiation was present.)
- EVA-A was usually the second-most affected material in the experiments. EVA-A demonstrated the greatest change in τ_{rsw} or YI in 2/16 experiments.
- The rank of the remaining materials for τ_{rsw} or YI often varied between EVA-D, EVA-B, and EVA-C.

- Inflections in transmittance or YI trends were sometimes observed for EVA-A, EVA-B, EVA-C, EVA-D, and TPU. The occurrence of an inflection and corresponding UV dose varied with the ChT used during weathering. Materials were more frequently affected and/or affected at a lesser *H* when ChT was increased. In contrast, many of the materials showed minimal degradation at the lowest ChT of 40°C or 45°C.
- EVA-E did not demonstrate a significant change in τ_{rsw} or YI in the study.

The results in Figure 3 and Figure 4 may be compared to the literature, which has historically focused on YI. Regarding the artificial weathering of EVA-A and EVA-B, Ref. [8] identifies a change in YI of ~56 that was observed for the STR product PHOTOCAP A9918P/UF (i.e., EVA-A), whereas a change in YI of ~30 was observed for 15295P/UF (i.e., EVA-B). Weathering exposures in Ref. [8] achieved a similar cumulative radiant exposure, but with a lower irradiance level (E_{340} of 0.55 $W \cdot m^{-2} \cdot nm^{-1}$) and higher applied temperature. The 100°C black-panel temperature in Ref. [8] would result in a sample temperature up to ~15°C–20°C higher than specimens in this study (verified at 66°C for participant 5).

Inflections as observed in the data profiles in Figure 3 and Figure 4 are generally associated with degradation modes occurring via multiple chemical mechanisms. Two different behaviors are noted here: in some cases, a steeper slope follows an initial period of more gradual sustained change; in other cases (e.g., EVA-D in Figure 4), a rapid degradation is observed in the early stages of exposure, followed by a more gradual degradation. The former case may result from the loss of a critical additive or sufficient generation of a more deleterious product species. The latter case may result from the initial depletion of a deleterious reactant species.

Some material-specific observations and conclusions can be made from the general results of the study. The following discussion will be reinforced by more-detailed examination of specific experiments, e.g., from the final transmittance spectra of the weathered specimens shown below. The more rapid and significant optical degradation of EVA-A is consistent with the literature (e.g., Ref. [28]) for that early-generation formulation. EVA-B, a subsequent generation formulation, however, shows notable improvement relative to EVA-A. The lesser durability of EVA-A suggests that interaction between Lupersol 101 peroxide and other additive(s) strongly contributes to discoloration. In Figure 3 and Figure 4, the replacement of Lupersol 101 with TBEC provides the notable improvement in EVA-B and the other formulations. The transmittance of EVA-C was observed to increase

with *H* in several experiments, which may result from the evolution of crystallinity in the material or the loss of additives with weathering. In some of the experiments at the greatest ChT, YI was reduced for EVA-C, suggesting that Naugard P causes some discoloration. EVA-D was found to rapidly discolor in many of the weathering experiments, suggesting that the Tinuvin 329 UV absorber is vulnerable to interaction with other additive(s). The change in YI for EVA-D stabilized in many of the experiments, suggesting that the other harmful additive species (such as the peroxide remaining after lamination) may have been depleted. The minimally affected and stable transmittance of EVA-E confirms that additive interactions with the UV absorber, i.e., Cyasorb UV-531 or Tinuvin 329, are the primary source of discoloration in the EVA formulations examined in this study. Based on the results, interactions between the UV absorber, curing agent, and/or antioxidant additives are suspected to contribute to discoloration. (The corresponding depletion of the UV absorber is explored in the examination of the spectra in Figure 9 and Figure 10, below). The TPU was the most acute indicator of UV weathering, including showing overt increases in discoloration with ChT. Little can be deduced about the origins of the degradation of the TPU because its formulation is not known. While the underlying chemistry enabling loss of transmittance was beyond the scope of this study, some examination of the effect of specific additives and interaction between some combinations of additives was recently reviewed in Ref. [16].

5.4 COMPARING ALL EXPERIMENTS IN THE STUDY

The results for all of the experiments are shown in Figure 5 for EVA-A and Figure 6 for EVA-B. Because the four hottest test conditions resulted in greater degradation, an inset (b) is provided in each figure to show the detail and provide labels for the remaining experiments. Error bars are not given in the figures, because the results of many experiments are presented. The variability of the measurements is, however, comparable to Figure 3, Figure 14, and Figure 15. The experiments performed at participant 4, where no irradiation was present, are included in Figure 5 and Figure 6; the cumulative duration of these experiments (in days) is indicated at the top axis of each figure. *H* is provided for the experiments where irradiation was applied for the wavelength range 295 nm $\leq \lambda \leq$ 360 nm. *H* varies between the experiments because of the different target intensity (Table III) as well as the spectral distribution of radiation (which varies with the source and filters used, Figure 1).

Regarding the results in Figure 5 and Figure 6, the relatively stable τ_{rsw} when no irradiation is present identifies that the degradation occurring in the remaining experiments results from UV degradation. That is, other factors,

including thermal and hydro degradation, are less significant than UV degradation through the range of conditions examined. Comparison of Figure 5 (for EVA-A, a known bad product) to Figure 6 (for EVA-B, an improved product) suggests that the limit of 2% might be applied for τ_{rsw} as an acceptance limit for the ChT of 60°C. The distinct separation between the experiments performed at the ChT of 80°C or 90°C identifies that UV degradation is thermally activated. The greater change in the four hottest experiments may suggests an alternate damage regime, e.g., where the kinetics are fundamentally affected by elevated temperature or the loss of formulation additives. The transmittance spectra will next be compared between key experiments to assess the mechanisms contributing to optical degradation when the UV source, ChT, and ChRH are varied.

5.5 EXAMINATION OF THE TRANSMITTANCE SPECTRA IN KEY EXPERIMENTS

The material-specific optical performance (hemispherical transmittance, τ_h {%}) spectra are shown in Figure 7 for all the material types aged by participant 5 using a Xe lamp for the applied conditions of E_{340} of 1.0 $W \cdot m^{-2} \cdot nm^{-1}$, ChT of 60°C, and ChRH of 50%. The transmittance of TPU and EVA-A is greatly *decreased* in the visible wavelengths above 400 nm. EVA-D is affected similarly, with a lesser magnitude of change. EVA-B and EVA-C are relatively unchanged through the experiment. The transmittance of EVA-E is *increased*, as its λ_{cUV} is shifted to shorter wavelengths with weathering. The hemispherical reflectance of silica is included in Figure 7 so that the optical absorptance might be estimated from the measured transmittance.

The change in the transmittance spectra for TPU and EVA-A is consistent with the decreased transmittance with weathering for these materials in Figure 3. The loss in transmittance for these materials comes with a significant increase in YI in Figure 4. The optical degradation for these materials may be explained by chromophore formation, e.g., from UV absorber, peroxide, and/or AO additives. The degradation of EVA-D is similar, including loss of transmittance and increased YI, and may also result from chromophore formation. The increased UV transmittance (below 400 nm) for EVA-E and EVA-C instead likely results from different reasons, including the loss of additive(s) or the evolution of crystallinity with age. Comparing Figure 7 to Figure 2, the phenolic anti-oxidant BHT is optically affecting from 250 nm to 290 nm, the same wavelength range where EVA-E is shifted by weathering. The optical effect of the Z6030 primer and TBEC curing agent were not examined in this study. For EVA-E, this is likely the result of the loss of a Careful observation of EVA-C in Figure 3 and Figure 4 identifies an increase in YI (usually associated with formation of new optically absorbing species) that

counter-intuitively occurs at the same time as an increase in transmittance. This is seen in the transmittance spectra in Figure 7 for aged EVA-C, where an increase in the spectral bandwidth below the λ_{cUV} occurs, along with a decrease in the transmittance above the λ_{cUV}. For EVA-C, the increase in τ_h below ~350 nm outweighs the reduced transmittance just above the λ_{cUV}. The extraction of soluble, low molecular weight additives (e.g., using gas chromatography-mass spectroscopy) for identification and analysis of -change concentration or -composition may be performed in a future study to better understand the mechanism(s) contributing to optical degradation.

The transmittance spectra are shown in Figure 8 for all the material types aged by participant 6 using a UVA-340 fluorescent chamber (E_{340} of 1.0 $W \cdot m^{-2} \cdot nm^{-1}$, ChT of 62°C, and ChRH of ~7%). Overt differences after weathering are observed for EVA-E and TPU. The spectral bandwidth of EVA-E is increased (decrease in the λ_{cUV} of 3 nm). Rounding of the cut-on profile for TPU is observed after weathering (original YI of 1.22 with a final YI of 13.7). The spectra of the remaining materials were not overtly changed with weathering, e.g., the YI of EVA-A and EVA-D was increased by <2 at the end of the experiment. Degradation from weathering in Figure 8 occurs to a lesser extent than in Figure 7, where rounding of the cut-on profile was observed for EVA-A and EVA-D. Compared to Ref. [18], the effects of weathering in Figure 8 are less than those for the UVA-340 chamber used by participant 5. In that experiment, the transmittance of EVA-A and TPU was greatly reduced above 400 nm, with a corresponding increase in YI. EVA-D was affected similarly, but to a lesser magnitude. The UV transmittance was increased in Ref. [18] for EVA-A, EVA-C, and EVA-E, with decreases in the λ_{cUV} of 64, 11, and 20 nm, respectively.

The degradation in Figure 8 for the UVA-340 chamber at participant 6 is less that than for the Xe chamber participant 5 in Figure 7, which gave less degradation than the UVA-340 chamber in Ref. [18] at participant 5. A critical difference for the UVA-340 chambers include the lesser irradiance at participant 6 (E_{340} of 1.0 $W \cdot m^{-2} \cdot nm^{-1}$) relative to that at participant 5 (E_{340} of 1.2 $W \cdot m^{-2} \cdot nm^{-1}$). A lesser irradiance at the same chamber temperature would be expected to reduce the rate of degradation. In contrast, the Xe chamber weathering performed at participant 5 in Figure 7 was run at the E_{340} of 1.0 $W \cdot m^{-2} \cdot nm^{-1}$ and a ChT of 60ºC. The greater visible and infrared irradiance for Xe sources in Figure 1 would be expected to give a greater specimen temperature. Increased specimen temperature for Xe chambers (from additional longer-wavelength radiation) would be expected to increase the rate of degradation. The greater degradation observed for EVA-A, EVA-C, and TPU in Ref. [18] for

a UVA-340 chamber may, however, suggest a photobleaching process enabled by the longer-wavelength radiation present in Xe chambers that reduces the population of chromophore species and subsequent optical damage. For EVA-C in Figure 7 and Ref. [18], the increase in τ_h at ~350 nm specifically facilitates the increase in its τ_{rsw} with age. Cyasorb UV-531 is the strongest-acting additive in Figure 2 for EVA-C at that wavelength.

The transmittance performance spectra are shown in Figure 9 for all the material types aged by participant 1 using a Xe chamber (E_{340} of 1.0 $W \cdot m^{-2} \cdot nm^{-1}$, ChT of 80°C, and ChRH of 30%) and Figure 10 for all the material types aged by participant 2 using a Xe chamber (E_{340} of 0.8 $W \cdot m^{-2} \cdot nm^{-1}$, ChT of 80°C, and ChRH of 20%). Overt differences after weathering are observed for all materials, including a rounding of the cut-on profile for EVA-A, EVA-B, EVA-C, EVA-D, and TPU, as well as an increased spectral bandwidth for EVA-E. The changes in Figure 10 are generally more significant than in Figure 9, with resulting greater reductions in τ_h as well as greater changes in λ_{cUV}.

The degradation for EVA-A and EVA-C, particularly the reduction in the λ_{cUV} in Figure 9 and Figure 10, suggests the loss of the UV absorber. In Figure 2, Tinuvin 329 and Cyabsorb UV-531 are the only additives with significant absorption from ~280–380 nm. The loss of these additives would explain the increased UV transmittance of EVA-A and EVA-C in Figure 9 and Figure 10. The steady λ_{cUV} for EVA-B in Figure 9 and EVA-D in Figure 9 and Figure 10 suggests that the UV absorber has not been as greatly depleted or that the absorption spectra of newly formed species absorb below λ_{cUV} in those experiments. The greater degradation observed in Figure 10 might not be expected based on the lesser E_{340} and ChRH used in that experiment. Participant 2, however, used a s-boro/quartz filter combination, which in Figure 1 provides greater UV radiation, including wavelengths not present in the terrestrial solar spectrum. The greater degradation in Figure 10 therefore is a reminder of the importance of the spectrum of the UV source, which in the IEC TS 62788-7-2 weathering standard must be compliant with ASTM D7869.

The optical performance spectra are shown in Figure 11 for all the material types aged by participant 4 using a dark chamber (E_{340} of 0.0 $W \cdot m^{-2} \cdot nm^{-1}$, ChT of 80°C, and ChRH of 30%). The data in the figure were obtained after remeasuring to verify final optical performance and extend the range of the results below 250 nm. For many materials, the final spectra for the weathered specimens are not distinguished from those of the unaged

specimens. Regarding the EVA formulations, only a slight discoloration (ΔYI of ~3 for EVA-D and ~1 for EVA-A and EVA-B) was observed with weathering. Some rounding of the UV cut-on profile was specifically observed for EVA-E. The effect on the spectral transmittance of EVA-E (occurring below 400 nm, with the corresponding ΔYI of <1) was to decrease the spectral bandwidth, opposite the trend shown for the aging of EVA-E in Figure 7, Figure 8, Figure 9, and Figure 10. A slight discoloration (ΔYI of ~4) was observed with time throughout the TPU specimens aged at 80°C. The maximum change in the λ_{cUV} of 2 nm is observed in Figure 11. The change in spectra for specimens weathered at participant 4 using a dark chamber was less than that in Figure 11 at the ChT of 60°C and 45°C, respectively (not shown).

The minimal changes in the spectra between the weathered and unaged condition in Figure 11 confirms that the changes in optical performance are primarily caused by UV photodegradation. Minimal formation of chromophore species (which would round the UV cut-on profile) or loss of formulation additives (which would shift λ_{cUV}) is suspected for the materials when no light was present during weathering. Figure 11 for the ChT of 80°C suggests that the evolution of crystallinity (e.g., with temperature) does not likely explain changes in transmittance in this study. A minor thermal degradation is, however, implied for the materials examined here, including EVA-A and TPU. A bleaching process is implied in Figure 11 for EVA-E, where the shift in UV cut-on profile is opposite to that in the experiments where irradiation is present. Bleaching, which typically breaks down chromophore species and increases spectral bandwidth, occurs in EVA-E when no light is present despite its λ_{cUV} being less than 250 nm.

5.6 ADDITIONAL RESULTS FROM SELECT EXPERIMENTS: VISUAL OBSERVATIONS

As shown in Figure 12, unique physical damage was observed in the hottest experiments, i.e., UV weathering performed at the ChT of 80°C or 90°C. The figure shows representative microscope images, including insets obtained at different magnifications. Round voids are seen at the periphery of the EVA-A specimen in Figure 12(a). A variety of sizes is observed for the voids in the inset images. The greatest population of voids was observed in the hottest experiments for EVA-A, with a lesser frequency for EVA-B, EVA-C, and EVA-D. Heterogeneous discoloration is seen within the EVA-B specimen in Figure 12(b). Although the greatest contrast is observed in Figure 12(b) at the periphery of the discolored region, other specimens in the study instead contained spots of reduced contrast within the central discolored region. A heterogeneous appearance was observed for

EVA-A, EVA-B, EVA-C, and EVA-D. The size of the discolored region was found to be formulation-specific within each experiment, e.g., compare EVA-A in Figure 12(a) and EVA-B in Figure 12(b). Linear voids are seen within the EVA-E specimen in Figure 12(c). Linear voids were only observed in EVA-E specimens weathered by participant 1 [~UVA-340 lamp, with E_{340} of 2.92 $W \cdot m^{-2} \cdot nm^{-1}$, ChT of 80°C, and ChRH of 50%. The specimens in Figure 12 were re-imaged after several months (not shown). No overt changes in the population of voids or the morphology of voids was observed when Figure 12 and subsequent images were compared.

A discolored central region is often described in the literature for EVA, where the clear periphery is attributed to photooxidative bleaching, which was recently verified to correspond to degradation favoring a balance of cross-linking rather than chain-scission [36]. In contrast, EVA-E did not discolor in the various experiments, whereas TPU was found to discolor throughout all affected specimens. The voids in the EVA materials may result from oxidation. The location within the photobleached periphery for the voids is generally consistent with the portion of the specimen where oxygen ingress is not diffusion-limited. The key factors contributing to the unique linear geometry in Figure 12(c) are not clear. EVA-E uniquely does not contain a UV absorber. The loss of material at the periphery resulted in a localized mechanical strain that could be visualized using cross-polarized imaging (not shown). The stable population and geometry of the voids over time, however, suggests that they formed during or shortly after weathering.

Voids similar to those in Figure 12 are not typically observed in PV installations, e.g., between cells or at the periphery of cells, where oxygen ingress is not diffusion-limited. This suggests that the voids in Figure 12 are damage that is not representative of historic PV modules. The majority of veteran modules studied to date feature a glass/backsheet construction and are rack-mounted or located in a moderate climate. The voids in Figure 12(a) and (c) may result from the greater temperature in the experiments, which might only be encountered on PV modules mounted on a roof, building façade, or other thermally insulating condition [38]. EVA-A was the most discolored material, giving it the greatest optical absorptance and therefore the greatest specimen temperature. This explains why it has the greatest density of voids between the materials. The damage in Figure 12 may also be unique to a glass/glass geometry, where no mechanically compliant backsheet is present. Because the specimens were cut from a larger laminate using a water-jet saw, the location of the bubbles is not attributable to edge pinch and tensile stress, but to perimeter ingress and/or egress of a chemical species. Voids and delamination

were also observed in glass/glass coupons subject to UV weathering in a study of encapsulation for concentrator PV [31].

Regarding the heterogenous discoloration in Figure 12, none of the specimens was internally cracked, which could facilitate photooxidative bleaching. Furthermore, the discolored region is located well within the specimens, so the heterogeneity cannot be explained by optical masking by the specimen holder or misalignment relative to the weathering chamber. The heterogeneous appearance may result from the lack of uniformity of formulation additives. For example, the heterogeneity of the cross-linking initiator was mapped in Ref. [37], where it was found to vary on the order of 50%. The heterogeneous appearance may also be subject to the evolution of the damage with time, e.g., where oxygen or moisture can quench free radicals to neutralize chromophore species.

5.7 ADDITIONAL RESULTS FROM SELECT EXPERIMENTS: FLUORESCENCE SPECTROSCOPY

The UV-VIS fluorescence spectra for EVA-C from select experiments is shown in Figure 13. The experiments include: participant 4 ("0/80/30", no irradiance, ChT of 80°C, and ChRH of 30%); participant 5 ("Xe 1.0/60/50", Xe lamp, with E_{340} of 1.0 $W \cdot m^{-2} \cdot nm^{-1}$, ChT of 60°C, and ChRH of 50%); participant 5 ("UVA-340 1.2/62/~7", UVA-340 lamp, with E_{340} of 1.2 $W \cdot m^{-2} \cdot nm^{-1}$, ChT of 62°C, and ChRH of ~7%); participant 5 ("Xe 1.0/90/20", Xe lamp, with with E_{340} of 1.0 $W \cdot m^{-2} \cdot nm^{-1}$, ChT of 90°C, and ChRH of 20%); and participant 2 ("Xe 0.8/80/20", Xe lamp, with E_{340} of 0.8 $W \cdot m^{-2} \cdot nm^{-1}$, ChT of 80°C, and ChRH of 20%). Complementary excitation spectra (dashed lines) and emission spectra (solid lines) are shown in Figure 13. The spectra are given in Figure 13 for the strongest emission peak observed in each experiment. The weakest-magnitude spectra are observed for 0/80/20 (participant 4); the strongest-intensity spectra are observed for 0.8/80/20 (participant 2). The spectra for 0/80/30, 1.0/60/50, and 1.2/62/~7 are self-similar in shape, whereas the spectra for 1.0/90/20 and 0.8/80/20 are self-similar to a different shape.

The profile of the fluorescence spectra results from the chemistry of the lumophore species present, whereas the intensity results from the concentration of the lumophore species. Regarding specific observations, the significant difference in intensity between dark weathering and the other spectra is consistent with photo-facilitated degradation, i.e., where lumophore species would not be expected for dark weathering. The spectra for Xe 1.0/60/50 and UVA-340 1.2/62/~7 are self-similar, implying that similar chemical species are being produced during weathering. The intensity of spectra for Xe 0.8/80/20 is greatest in Figure 13, implying it is the greatest net

rate of lumophore formation. The rank order (Xe 0.8/80/20 > Xe 1.0/90/20) is consistent with Figure 6 but opposite to Figure 5. In weathering, however, the rank order of degradation may vary with the formulation.

Regarding general observations, the intensity of the spectra for UVA-340 1.2/62/~7 is noticeably greater than Xe 1.0/60/50 despite a 20% difference in the irradiance intensity. Furthermore, the intensity of the spectra for Xe 0.8/80/20 is greater than that of Xe 1.0/90/20, despite the greater irradiance intensity and ChT used in Xe 1.0/90/20. This may result from the different UV spectra used in the experiments, i.e., unfiltered UVA-340 source for UVA-340 1.2/62/~7; D7869/quartz-filtered Xe source for Xe 1.0/60/50 and Xe 1.0/90/20; and s-boro/quartz-filtered Xe source for Xe 0.8/80/20. This implies that UVA-340 and s-boro/quartz-filtered Xe do not give a rate of degradation consistent with the law of reciprocity relative to D7869/quartz-filtered Xe.

The self-similar spectra for 0/80/30, 1.0/60/50, and 1.2/62/~7 in Figure 13 imply a similar chemistry of product species and corresponding enabling chemistry that is different from the chemistry in 1.0/90/20 and 0.8/80/20. The disparity between the fluorescent intensity of the hottest experiments and that of the other experiments is consistent with Figure 5 and Figure 6, where a significantly greater degradation in transmittance is observed for the hottest four experiments, i.e., ChT ≥80 ºC. The disparity between the fluorescent spectra for Xe 1.0/90/20 and Xe 0.8/80/20 relative to the other experiments is consistent with Figure 12, where voids were observed for the hottest four experiments, i.e., ChT ≥80 ºC. The fluorescence characterization therefore implies an alternate damage regime for the hottest experiments. An alternate damage regime may be enabled for reasons including: the loss of additive species during weathering; a kinetically enabled transition between competing enabling chemistries; a change in the degradation kinetics enabled by a phase transition; or the autocatalysis of the material from product species.

5.8 ACTIVATION ENERGY FROM THE ARRHENIUS ANALYSIS

The results of three experiments at participant 1, which serve as the basis for an Arrhenius analysis, are summarized in Figure 14 and Table V. The change in τ_{rsw} for EVA-A is shown in Figure 14, where H is determined for 295 nm ≤ λ ≤ 360 nm so that the results may be readily compared to Figure 3, Figure 5, and Figure 6. As indicated in Figure 14, a linear best-fit (indicated with a line in the figure) was applied up to an inflection in the data. Data occurring after an inflection are indicated in Figure 14 where only markers are present. Although most materials were fit to the origin, EVA-D was analyzed after its initial stabilization from weathering, e.g., $H > 0.1$

GJ·m^2 for EVA-D in Figure 4. The Arrhenius analysis and corresponding linear fit for EVA-A are shown in the inset of Figure 14. The test conditions are labeled in the inset, where each data point follows from the slope of the fit in Figure 14. The verified specimen temperature, determined using an additional coupon with an embedded thermocouple, is shown in the inset. The melt transition temperature of 56.4ºC ("T_m", the average measured for the EVAs in this study) is also indicated in the inset.

The results of the analysis represented in Figure 14, are summarized for all materials in Table V, including the frequency factor, c_1 {dimensionless}, and the activation energy, E_a {kJ·mol^{-1}}. The characteristics of τ_{rsw} and YI were analyzed separately. Unlike Figure 14, the analysis in Table V was performed where H was determined for the wavelength of 340 nm, i.e., used as the controlling wavelength in most commercial weathering chambers. Based on the negligible change in τ_{rsw} and YI in the experiments, a valid positive E_a value could not be obtained for EVA-E; therefore, it is not considered in Table V, indicated "N/A." Like Figure 14, variability is indicated in Table V for two S.D.

An activation energy on the order of 30–60 kJ·mol^{-1}is estimated in Table V for the loss in τ_{rsw} and increased YI of the EVA and TPU materials. The E_a and its variation was generally similar for each material between τ_{rsw} and YI. The range of 10–40 kJ·mol^{-1}is typically observed for the photodegradation of structural polymers and coatings [34]. The activation energies in Table V are therefore consistent with defect-mediated degradation, facilitated by additive interactions or impurities. The shape of the fit in the inset of Figure 14 profile is generally linear, but with a downward concavity. This implies there is no overt change in the rate of degradation through the temperature range and cumulative UV dose (i.e., up to any data inflections) examined. Additional intermediate data points would help to confirm the concavity in the inset of Figure 14 and to better ascertain if the melting of EVA contributes to the rate of degradation above T_m. It should be noted that the effect of a phase transition on degradation rate is not well established for PV polymers. In comparison to T_m, maximum annual temperatures from 65°C–85°C are anticipated within rack- and roof-mounted modules in hot, dry locations [38]. Furthermore, the weathering in this study occurs where the specimen temperature is maintained in steady state relative to the glass and phase transition temperatures, whereas as the complex diurnal time-temperature history of a PV modules may facilitate a different evolution of crystallites within the EVA, including differences in population, composition and geometry.

One additional factor that could contribute to error in Figure 14 and Table V follows from radiant heat transfer. Irradiated discolored specimens would be expected to rise to greater temperature based on their enhanced optical absorptance. Because the rate of degradation is shown in Table V to be thermally coupled, discoloration could accelerate degradation and the loss of transmittance through the experiments. The specimen temperature, verified using an additional coupon specimen with an embedded thermocouple, is expected to be most accurate at the start of the experiment, where the effect of UV-induced discoloration would be minimal. The analysis procedure here, however, should reduce the aforementioned effects of interaction between discoloration and radiant heat transfer. The linear fits, shown in Figure 14 for example, should moderate the effects of discoloration-accelerated degradation. The results in Table V apply to degradation occurring prior to an inflection in τ_{rsw} or YI, which limits the data considered to the maximum τ_{rsw} of 2%–3%. Less optical absorption and subsequent specimen temperature rise would therefore be expected in Table V than at the end of the hottest experiments in Figure 5.

5.9 DEGRADATION RATE ANALYSIS OF THE EFFECT OF WATER

The results of two experiments are compared between participant 1 and participant 5 in Figure 15 and Table VI, where all chamber conditions were nominally identical (Xe lamp, with E_{340} of 1.0 $W \cdot m^{-2} \cdot nm^{-1}$ and ChT of 60°C) other than the ChRH (30% or 50%). A linear degradation rate analysis was applied between the experiments to assess the effect of moisture on weathering. The change in τ_{rsw} for EVA-A and TPU is shown in Figure 15, where H is determined for 295 nm ≤ λ ≤ 360 nm so that the results may be readily compared to Figure 3, Figure 5, and Figure 6. Data points in the figure are connected with a line to guide the eye and distinguish between the materials and the experiments.

The results of the analysis in Figure 15 are summarized in Table VI. As in the Arrhenius analysis in Figure 14 and Table V, a linear fit was applied to each material from $H = 0$ up to any perceived inflection in the $\Delta\tau_{rsw}$ or ΔYI data. In the analysis, most materials were fit to the origin ($\Delta\tau_{rsw}$ of 0), whereas EVA-D was analyzed after its initial stabilization from weathering, e.g., $H > 0.1$ GJ·m^2 in Figure 4. The degradation factor, k_H {dimensionless}, is taken as the ratio of the slope of the trend-line fit for the experiment at 50% RH to the slope obtained for the experiment at 30% RH. As in Table V, the analysis in Table VI was performed where H was determined for the wavelength of 340 nm. k_H is given in Table VI, where an overt trend with H could be observed in both experiments. For example, the negligible change in τ_{rsw} and YI in the experiments for EVA-E could not justify a valid linear

fit, indicated "N/A." The k_H values for the EVA materials were typically less than one, whereas the values for TPU were at or above unity.

The results in Figure 15 and Table VI suggest that the reduction in transmittance and increase in discoloration with UV weathering will be greater for EVA in a dry environment. This suggests that hot, dry locations would give a greater degradation rate than hot, humid locations. No significant difference was observed between experiments for TPU, suggesting a neutral dependence over the humidity range examined here. No additional characterization was performed to identify if the rate of production of chromophore species was reduced by moisture or if instead the subsequent neutralization of chromophores after weathering contributes to the results in Figure 15 and Table VI. Although the cursory examination here suggests a trend, the study would benefit from the examination of a greater range and number of RH values.

The study of the ingress of water lends perspective to Figure 15 and Table VI relative to the PV application. Ref. [39] describes analysis identifying that water diffusion through a 25 mm distance (the half-size of the glass/encapsulant/glass geometry coupons in this study) will occur in a few hundred hours in Damp Heat (85°C/85 %RH) and other accelerated tests (empirically confirmed in Ref. [40]), whereas moisture equilibration to 25 mm will take place on the front of a PV module (glass/encapsulant/cell geometry) on the order of a year in Bangkok, one of the most hot & humid terrestrial locations. Based on Refs. [39], [40], [41], [42], the specimens in this study were conditioned to a moisture concentration similar to their steady state condition prior to the 4000 hour cumulative experiments and stored in damp chambers to maintain their internal concentration of water when not being examined at readpoints. The ingress of oxygen may instead be directly assessed from the visual discoloration of the EVA in Figure 12 [36].

6. DISCUSSION

The results of this study can be qualitatively compared to assess the factors applied during artificial weathering. The discussion here, including the factors of irradiance, temperature, and moisture, is included to remember important considerations identified in this study. Figure 11 confirms that the degradation in this study results from optical irradiation, making it arguably the most significant factor. Furthermore, the inadvertent use of a s-boro/quartz filter combination by participant 2 gave greater degradation relative to the higher irradiance and/or temperature in other experiments in Figure 5 and Figure 6. Previously reported disparity in degradation also identifies that UVA-340 fluorescent sources can weather specimens differently than Xe sources [18]. That

study suggests that the use of fluorescent sources should be verified relative to Xe sources or natural weathering. The aforementioned examples, including different source types or filters, identify that fidelity relative to the terrestrial solar spectrum can be critical to the weathering of PV encapsulants. This consideration contributed to the designated use of a Xe source (filtered according to ASTM D7869) in IEC TS 62788-7-2.

The extreme degradation for the hottest experiments, including an alternate weathering regime in Figure 5 and Figure 6, identifies that temperature is also a significant contributor to degradation. Table V further quantifies the activation energy. The coupling with temperature importantly suggests that the temperature in the PV application should be considered relative to the specimen temperature used in weathering. It is encouraged to verify the specimen temperature during artificial weathering—particularly because the temperature control may vary between the make and models of commercial weathering equipment. In the case of natural weathering, for example, a black or heated substrate may be used with a transparent coupon specimen to achieve a specimen temperature similar to that in a module.

Humidity was found to affect degradation in Figure 15, where the extent of influence is not as overt as for temperature. It should also be remembered that the comparison here is limited to the range of conditions examined in the study. The limited examination in this study therefore does not provide a strong perspective on which is the potentially most damaging environment—a hot/dry or hot/humid location. It also remains to be clarified if elevated humidity reduced discoloration during weathering or after weathering, e.g., through the quenching of free-radical species.

The mechanisms enabling the greater degradation in the hottest experiments remain to be determined. For example, it is presently unclear if the melt-phase transition for EVA contributes by aiding the out-diffusion of additives, if the kinetics of competing enabling reactions, or the autocatalysis of the material from product species enable the alternate damage regime for the hottest experiments. It should be remembered that a limited number of EVA formulations were examined in this study. The initial results (preceding any inflection in the transmittance or YI) for the ChT of 60 °C importantly remain to be validated because they occur above the T_m for EVA. Feedback regarding the design of an accelerated test for an application with known time-temperature history both above and below a phase transition will be helpful to other industries. It remains to be established if a more complex weathering test is required, with time spent at temperature above and below the T_m. The results in the hottest

experiments (where an alternate weathering regime was observed) also remain to be verified for other EVA formulations or other base encapsulation materials.

Analysis of PV module temperature lends perspective to the results for the hottest experiments. As in Ref. [38], empirical models (e.g., the King model [43]) may be used with typical meteorological year (TMY3) data [44] to estimate module temperature. The accuracy of the King model is estimated to be on the order of ±5°C [35]. In Ref. [38], the temperature of 65°C (taken as a proxy for the specimen temperature for the ChT of 60°C) was estimated to approach the 97th percentile of the time-temperature distribution, occurring for rack-mounted glass/glass modules for 102 and 173 hours per TMY3 in Phoenix and Riyadh, respectively. Similarly, the temperature of 85°C (for the ChT of 80°C) was never estimated to occur for rack-mounted glass/glass modules, but was estimated to approach the 96th percentile of the time-temperature distribution, occurring for glass/backsheet modules with an insulated back for 250 and 284 hours per TMY3 in Phoenix and Riyadh, respectively. The nominal ChT of 60°C and subsequent specimen temperature of 65°C for six months of artificial weathering approximates the cumulative thermal history through a 25-year application life at their hottest temperatures for rack-mounted modules. The hottest module temperatures (65°C or 85°C) are, however, achieved intermittently in the PV application, whereas they are applied continuously in this study.

Recommendations for the artificial weathering of transparent coupon specimens can be provided relative to the previous estimates of module operating temperature. Rack-mounted glass/glass modules are presented as an example of utility PV, i.e., much of the PV presently installed throughout the world. A glass/glass geometry is chosen to give a conservative estimate, because it was found to give temperatures hotter than a glass/backsheet geometry in Ref. [43]. Based on the estimated operating temperatures as well as the results of the study here, it is suggested that the artificial weathering of transparent coupon specimens using a chamber temperature on the order of 60°C be applied to represent PV modules used in typical operating conditions, including location climate and mounting configuration. In this case, the A3 weathering condition from IEC TS 62788-7-2 (ChT of 65°C) might be applied for weathering. Lacking field validation, the A3 weathering condition is identified here rather than A2 (ChT of 55°C) to give a greater acceleration to the test. Because the IEC TS 62788-7-2 standard was only recently introduced, it is recommended to validate the A3 test condition relative to natural weathering, e.g., by identifying the acceleration factor for the test relative to benchmark locations. A glass/backsheet geometry with an insulated-

back might be used to represent modules in the hottest possible operating conditions, e.g., building-integrated PV. The previous estimates suggest that these modules may achieve temperatures in desert locations that are 20°C hotter than typical PV. Although a specimen temperature on the order of 80°C may be observed in PV, an alternate degradation regime was observed for the hottest experiments in this study. Therefore, it is recommended to confirm the validity of the alternate weathering regime for naturally weathered modules before an artificial weathering test condition can be confidently identified, e.g., condition A4 or A5 in IEC TS 62788-7-2.

The results in this study can be used to provide guidance for an acceptance limit for the change in optical performance in an accelerated test. Assuming ideal 8-hour-long UV days in the field, the cumulative radiant exposure for the nominal irradiance in the study here (1.0 $W \cdot m^{-2} \cdot nm^{-1}$ at 340 nm) would provide a 3.5-year equivalent dose of total UV for the AM1.5G spectrum [26] in Phoenix, AZ [45]. In contrast, the degradation rate for short-circuit current, I_{sc}, on the order of 0.25 to 0.33 $\% \cdot y^{-1}$ from encapsulant discoloration has been estimated for silicon PV modules [1,46,47]. Assuming a constant linear degradation, a loss in performance on the order of 2% might be expected after 6 to 8 years of field use. The proposed 2% performance criteria would allow modest acceleration from irradiation intensity and temperature, i.e., a 3.5-year equivalent artificial UV dose might be applied to mimic 8 years of field degradation. For example, the use of silica glass in this study provides an inherent acceleration of weathering because the glass transmits wavelengths of UV light that may be attenuated by PV front glass. The extent of acceleration would depend on the action spectrum of the encapsulation material [19]. The loss of transmittance of 2%, proposed as an acceptance limit, would apply to the early life of a PV module constructed using improved EVA (e.g., EVA-B as in Figure 6) and weathered similar to the nominal test conditions in this study (1.0 $W \cdot m^{-2} \cdot nm^{-1}$ at 340 nm, ChT of 60°C, and ChRH of 30% RH).

Activities including standards development and application-specific analysis have benefitted from this study. The PV packaging-materials weathering standard, IEC TS 62788-7-2 [23], was under development during this study. For example, the ChT was considered the development of the IEC TS 62788-7-2. The IEC 62788-1-7 standard is presently being developed to apply UV weathering of transparent PV packaging materials. IEC 62788-1-7 would apply the methods developed in this study for the weathering of encapsulants, frontsheets, and transparent backsheets. The repeatability and reproducibility of UV weathering is of concern to the PV community and is presently being examined in a follow-up Task Group 5 study.

The results of the study here could be applied to predict performance degradation and identify encapsulant product requirements. For example, the activation energies in Table V could be applied in an analytic model that considers the location-specific annual equivalent temperature and weighted-average relative humidity [48]. A numeric model that uses the activation energy and site-specific irradiance-temperature-humidity history to predict PV performance degradation has already been demonstrated [49]. Because a degradation analysis and its related considerations constitutes its own study, it is not explored here.

7. CONCLUSIONS

The degradation in optical performance for PV encapsulant materials was examined as a function of artificial UV weathering. The irradiance spectrum, chamber temperature, and chamber humidity were varied in a series of experiments examining six encapsulants. Key results include the following:

Minimal degradation was observed with no radiation present, confirming that the discoloration and optical performance degradation of EVA encapsulant results from UV degradation. **The highest-fidelity results are expected for UV sources replicating the terrestrial environment, e.g., as specified in ASTM D7869.** The use of an s-boro/quartz filter with a xenon source as well as the use of a UVA-340 fluorescent source were both found to affect degradation mechanisms, confirming the importance of the source spectrum used during weathering. The coupling between degradation and temperature was quantified using an Arrhenius representation. The study of the factor of temperature reminds us that it is important to consider the temperature in the PV application relative to the specimen temperature used during weathering. Although increased humidity was found to decrease discoloration, it remains to be determined if the effect primarily follows from the water-induced neutralization of chromophore species. The additive-specific durability of the materials here identifies that the majority of the degradation is specific to the formulation, rather than being intrinsic to the base EVA resin. The negligible discoloration observed for the EVA formulation containing no UV absorber specifically identifies that much of the loss in optical performance in this study results from the UV absorbers. A 2% loss in performance is suggested here to screen for acceptable encapsulant materials using artificial weathering. Correlation between the artificial weathering here and natural weathering of PV modules remains to be established, but it is expected to apply to the early years of module life.

An alternate weathering regime was identified for the hottest experiments in this study, i.e., chamber temperature of 80°C or greater. This regime is inferred from: 1) the inflection observed with UV dose

for the characteristics of transmittance and yellowness index; 2) the loss of the UV absorber additive, deduced from transmittance spectra; 3) the formation of voids at the periphery of the specimens subject to the hottest weathering; and 4) the disparate fluorescence spectra observed for the specimens subject to the hottest weathering. The enabling factor(s) for the alternate weathering regime in the hottest experiments remain to be determined, but they could include: 1) the out-diffusion and/or breakdown of formulation additives; 2) the melt-phase transition occurring in the EVA material resin; 3) the competing kinetics between different enabling chemical reactions; or 4) the autocatalysis of the material from product species. Although it remains to be validated and correlated with natural weathering, it is suggested that the artificial weathering of transparent coupon specimens using a chamber temperature on the order of 60°C may be applied for PV modules used in typical operating conditions (climates and mounting conditions). A follow-on study will be used to explore the feasibility of hotter weathering conditions, e.g., for PV modules used in hot operating conditions.

Activation energies on the order of 50 kJ·mol^{-1} were determined here. The activation energies observed in this study are consistent with defect-mediated degradation, facilitated by additive interactions and/or impurities. The results of the study here will be applied to define and interpret industry standards for the UV weathering of PV packaging materials, including IEC TS 62788-7-2 and IEC 62788-1-7. The study here importantly remains to be quantitatively correlated against natural weathering.

8. ACKNOWLEDGMENTS

The authors are grateful to: Kate Baughman, Dr. Matt Gray, Kaan Korkmaz, Byron McDanold, Ian Tappan, Rob Tirawat, and Ryan Willis. The authors would also like to thank the numerous members of the International Photovoltaic Quality Assurance Task Force (PVQAT) Task Group 5, who contributed to the design, execution, and analysis of this study. This work was authored [in part] by Alliance for Sustainable Energy, LLC, the manager and operator of the National Renewable Energy Laboratory for the U.S. Department of Energy (DOE) under Contract No. DE-AC36-08GO28308. Funding was provided by the U.S. DOE Office of Energy Efficiency and Renewable Energy (EERE) under the Solar Energy Technologies Office (SETO) under agreement number 30308. The views expressed in the article do not necessarily represent the views of the DOE or the U.S. Government. Instruments and materials are identified in this paper to describe the experiments. In no case does such identification imply recommendation or endorsement by NIST or NREL. The U.S. Government retains and the publisher, by accepting the article for publication, acknowledges that the U.S. Government retains a

nonexclusive, paid-up, irrevocable, worldwide license to publish or reproduce the published form of this work, or allow others to do so, for U.S. Government purposes.

9. REFERENCES

1. D.C. Jordan, S.R. Kurtz, K. VanSant, J. Newmiller, “Compendium of photovoltaic degradation rates,” PIP, 24(7), 978–989, 2016.
2. “IEC 61730-2 Photovoltaic (PV) module safety qualification – Part 2: Requirements for testing,” Edition 2, International Electrotechnical Commission: Geneva, 1–57, 2016.
3. “IEC 61215-2 Terrestrial photovoltaic (PV) modules – Design qualification and type approval,” Edition 1, International Electrotechnical Commission: Geneva, 1–41, 2016.
4. S. Fowler, X.H. Gu, D.C. Miller, N.H. Phillips, “PVQAT TG5: ‘UV weathering standards development within the PV industry,’” Proc. NREL PV Module Reliability Workshop (Golden, Colorado), 2017.
5. “ASTM D7869-17 Standard Practice for Xenon Arc Exposure Test with Enhanced Light and Water Exposure for Transportation Coatings,” ASTM International, West Conshohocken, PA, 1–10, 2017.
6. A.W. Czanderna, F.J. Pern. “Encapsulation of PV modules using ethylene vinyl acetate copolymer as a pottant: A critical review,” SOLMAT, 43, 101–181, 1996.
7. W.W. Holley, S.C. Agro, “Advanced EVA-based encapsulants: Final report,” NREL, Golden, CO, Rep. NREL/SR-520-25296, 1998.
8. C.G. Reid, et al., “UV aging and outdoor exposure correlation for EVA PV encapsulants,” Proc. SPIE, 8825–7, 2013.
9. A.L. Rosenthal, C.G. Lane, “Field-test results for the 6 MW Carrizo Solar Photovoltaic Power-Plant,” Solar Cells, 30, 563–571, 1991.
10. J.H. Wohlgemuth, R.C. Petersen, "Reliability of EVA modules", Proc. IEEE PVSC, 1993, 1090-1094.
11. D.C. Miller, M.T. Muller, M.D. Kempe, K. Araki, C.E. Kennedy, S.R. Kurtz, “Durability of polymeric encapsulation materials for concentrating photovoltaic systems,” Progress in Photovoltaics: Research and Applications, 21(4), 631–651, 2013.
12. F.J. Pern, A.W. Czanderna, “Characterization of ethylene vinyl acetate (EVA) encapsulant: Effects of thermal processing and weathering degradation on its discoloration,” Solar Energy Solar Mater., 25, 3–23, 1992.
13. F.J. Pern, “Luminescence and absorption characterization of ethylene-vinyl acetate encapsulant for PV modules before and after weathering degradation,” Polym. Deg. Stab., 41, 125–139, 1993.
14. N.S. Allen, M. Edge, M. Rodriguez, C.M. Liauw, E. Fontan, “Aspects of the thermal oxidation, yellowing and stabilization of ethylene vinyl acetate copolymer”, Polym. Deg. Stab. 2001; 71: 1-14.
15. N.S. Allen, M. Edge, M. Rodriguez, C.M. Liauw, E. Fontan, “Aspects of the thermal oxidation of ethylene vinyl acetate copolymer”, Polym. Deg. Stab. 2000; 68: 363-371.
16. C. Peike, L. Purschle, K.-A. Weiss, M. Köhl, M. Kempe, “Towards the origin of photochemical EVAS discoloration,, Proc. IEEE PVSC, 2013, 1579–1584.

17. F. Rummens, K. De Keyser, “How weathering tests on properly designed coupons can increase the service life of photovoltaic modules,” Sun Spots, 46(99), 1–8, 2016.
18. D.C. Miller, E. Annigoni, A. Ballion, J.G. Bokria, L.S. Bruckman, D.M. Burns, C. Chen, L. Elliott, L. Feng, R.H. French, S. Fowler, X.H. Gu, P.L. Hacke, C.C. Honeker, M.D. Kempe, H. Khonkar, M. Köhl, L.-E. Perret-Aebi, N.H. Phillips, K.P. Scott, F. Sculati-Meillaud, T. Shioda, S. Suga, S. Watanabe, J.H. Wohlgemuth, “Degradation in PV encapsulation transmittance: An interlaboratory study towards a climate-specific test,” Proc IEEE PVSC, 972, 2015.
19. D.C. Miller, M.D. Kempe, C.E. Kennedy, S.R. Kurtz, “Analysis of transmitted optical spectrum enabling accelerated testing of multi-junction CPV designs,” Optical Engineering, 50(1), 013003, 2011.
20. Ed. D.V. Rosato, R.T. Schwartz, Environmental effects on polymeric materials, John Wiley and Sons: New York, 1968.
21. J.W. Martin, J.W. Chin, T. Nguyen, “Reciprocity law experiments in polymeric photodegradation: A critical review,” Prog. Organic Coat., 47, 292–311, 2003.
22. K.P. Scott, H.K. Hardcastle, “A new approach to characterizing weathering reciprocity in xenon arc weathering devices,” In Service Life Prediction of Polymeric Materials. Springer: New York, 2009.
23. “IEC TS 62788-7-2 Measurement procedures for materials used in photovoltaic modules – Part 7-2: Environmental exposures – Accelerated weathering tests of polymeric materials,” International Electrotechnical Commission: Geneva, 1–26, 2017.
24. S. Fowler, “Developing steady state exposure conditions in an ASTM G154 fluorescent UV test chamber for backsheet materials,” Proc. NREL PVMRW, 2014.
25. “ASTM G154-16 Standard Practice for Operating Fluorescent Ultraviolet (UV) Lamp Apparatus for Exposure of Nonmetallic materials,” ASTM International, West Conshohocken, PA, 1–11, 2016.
26. “IEC 60904-3 Photovoltaic devices – Part 3: Measurement principles for terrestrial photovoltaic (PV) solar devices with reference spectral irradiance data,” International Electrotechnical Commission: Geneva, 1–200, 2016.
27. G.P. Smestad, L. Micheli, T.A. Germer, E.F. Fernández, “Optical characterization of PV glass coupons and PV modules related to soiling losses,” in review.
28. “IEC 62788-1-4 Measurement procedures for materials used in photovoltaic modules – Part 1-4: Encapsulants – Measurement of optical transmittance and calculation of the solar-weighted photon transmittance, yellowness index, and UV cut-off wavelength,” International Electrotechnical Commission: Geneva, 1–37, 2016.
29. D.C. Miller, J. Apezteguia, J.G. Bokria, M. Köhl, N.E. Powell, M.E. Smith, M.D. White, H.R. Wilson, J.H. Wohlgemuth, “Examination of an optical transmittance test for photovoltaic encapsulation materials,” Proc SPIE, 8825–8, 2013.
30. “Chapter 7: Ultraviolet spectrometry,” in Silverstein RM, Bassler GC, Morrill TC. Spectrometric Identification of Organic Compounds: Fifth Edition. John Wiley and Sons Inc.: New York, 1991.

31. D.C. Miller, M.D. Kempe, M.T. Muller, M.H. Gray, K. Araki, S.R. Kurtz, “Durability of polymeric encapsulation materials in a PMMA/glass concentrator photovoltaic system,” Progress in Photovoltaic, 24, 1385–1409, 2016.
32. J.A. Simms, “Acceleration shift factor and its use in evaluating weathering data,” J. Coat. Technol., 59(748), 45–53, 1987.
33. K.T. Gillen, R.L. Clough, “Time-temperature-dose rate superposition: A methodology for extrapolating accelerated radiation aging data to low dose rate conditions,” Polym. Deg. Stab., 24, 137–168, 1989.
34. J.E. Pickett, D.A. Gibson, M.M. Gardner, “Effects of temperature on the weathering of engineering thermoplastics,” Polym. Deg. Stab., 93, 684–691, 2008.
35. M.D. Kempe, D.C. Miller, J.H. Wohlgemuth, S.R. Kurtz, J.M. Moseley, Q. Shah, G. Tamizhmani, K. Sakurai, M. Inoue, T. Doi, A. Masuda, S.L. Samuels, C.E. Vanderpan, “Field testing of thermoplastic encapsulants in high temperature installations,” Energy Science and Engineering, 3(6), 565–580, 2015.
36. M.D. Kempe, D.C. Miller, J.H. Wohlgemuth, S.R. Kurtz, J.M. Moseley, D.L. Nobles, K.M. Stika, Y. Brun, S.L. Samuels, Q. Shah, G. Tamizhmani, K. Sakurai, M. Inoue, T. Doi, A. Masuda, C.E. Vanderpan, “Multi Angle Laser Light Scattering Evaluation of Field Exposed Thermoplastic Photovoltaic Encapsulant Materials”, Energy Sci. Eng., 4 (1), 2016, 40-51.
37. S.-H. Schulze, M. Pander, S. Dietrich, M. Ebert, “Encapsulation polymers – A key issue in module reliability,” PV. Intl, 118–126, 2011.
38. D.C. Miller, M.D. Kempe, S.H. Glick, S.R. Kurtz, “Creep in photovoltaic modules: Examining the stability of polymeric materials and components,” Proc. IEEE PVSC, 262–268, 2010.
39. M.D. Kempe, J.H. Wohlgemuth, "Equating Damp Heat Testing with Field Failures of PV Modules", Proc. IEEE PVSC, 2013.
40. M.D. Kempe, A.A. Dameron, M.O. Reese, "Evaluation of moisture ingress from the perimeter of photovoltaic modules", PIP, 22, 2014, 1159–1171.
41. M.D. Kempe, "Modeling of rates of moisture ingress into photovoltaic modules", SOLMAT, 90, 2006, 2720–2738.
42. M.D. Kempe, J.H. Wohlgemuth, "Evaluation of Temperature and Humidity on PV Module Component Degradation", Proc. IEEE PVSC, 2013.
43. D.L. King, W.E. Boyson, J.A. Kratochvil, “Photovoltaic array performance model,” SAND2004-3535, 1–43, 2004.
44. http://rredc.nrel.gov/solar/old_data/nsrdb/1991-2005/tmy3/
45. http://atlas-mts.com/online-tools/weather-summary-reports/
46. D.C. Jordan, J.H. Wohlgemuth, S.R. Kurtz, “Technology and climate trends in PV module degradation,” Proc. Euro PVSEC, 2012.
47. D.C. Jordan, T.J. Silverman, B. Sekulic, S.R. Kurtz, “PV degradation curves: non-linearities and failure modes,” Proc. Euro. PVSEC Conf., 2016.
48. Kempe M.D., “Evaluation of the uncertainty in accelerated stress testing,” Proc PVSC, 614, 2014.

49. S.-Y. Oh, W.-S. So, M.-S. Kim, J.H. Jung, J.-H. Park, “Simulations and benchmarks of the outdoor UV degradation of EVA using the SOlar REliability Simulator (SORES),” Proc. PV Module Reliability Workshop, 2018, Xxx.

Figures:

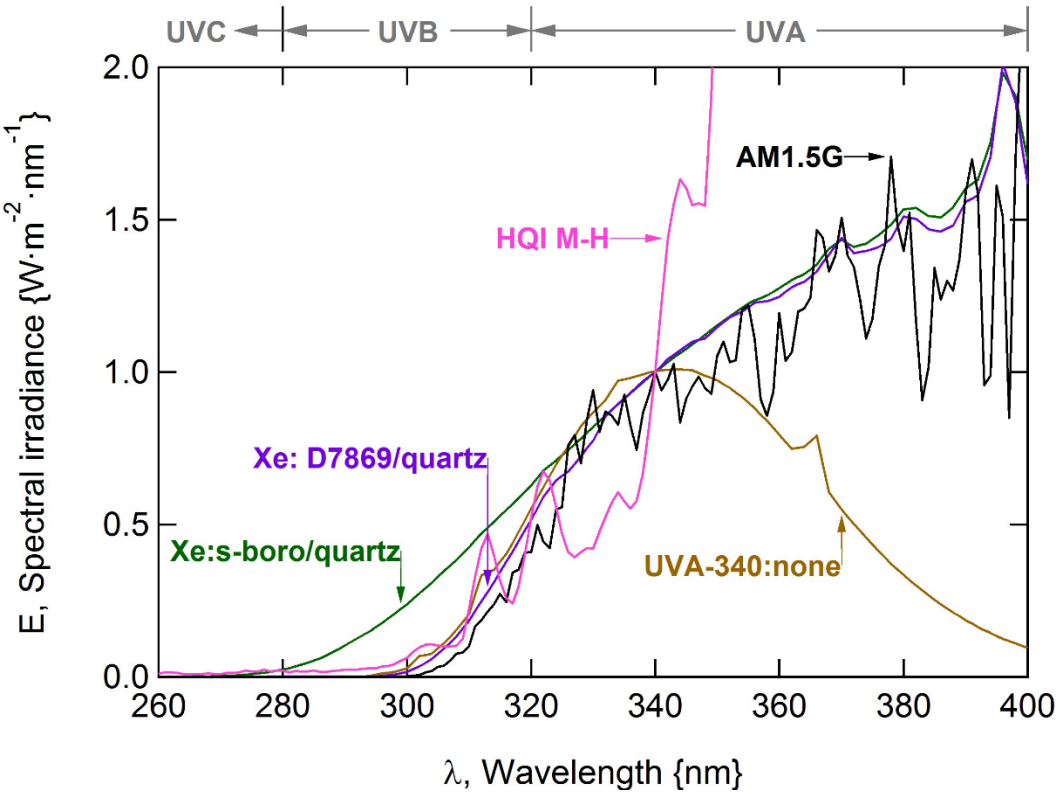

Figure 1: Overlay of the UV spectra from source/filter combinations used in the study. All spectra have been normalized to the E_{340} of 1.0 W·m^{-2}·nm^{-1} so that the spectral content may be compared. The colloquial UV waveband designations are indicated at the top of the figure.

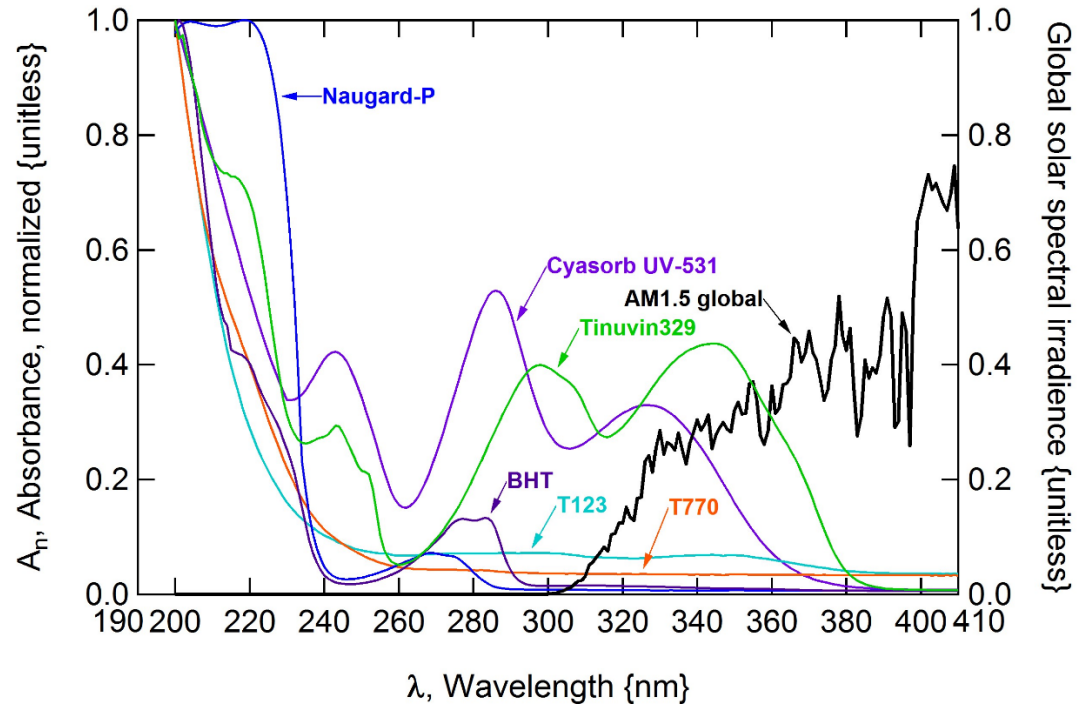

Figure 2: The optical absorptance of the additives (in Table II, in ~0.01% wt. hexane solution) shown relative to the terrestrial AM1.5G solar spectrum (normalized to its peak at 495 nm).

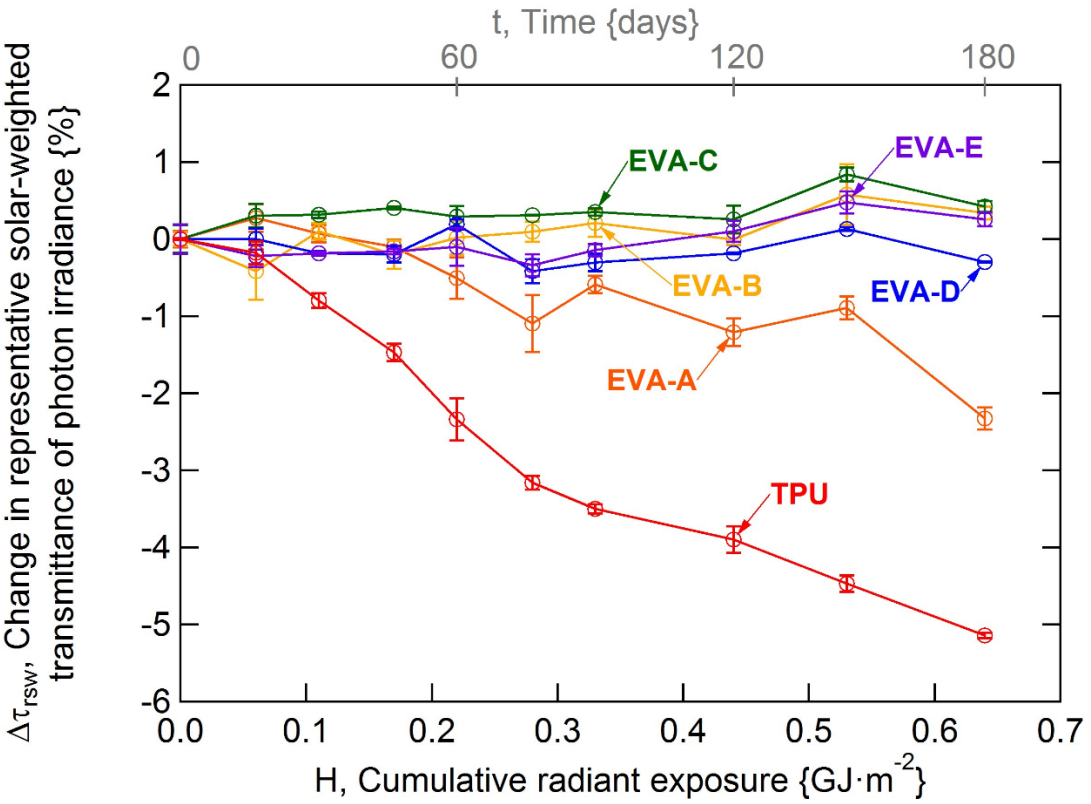

Figure 3: Change in transmittance with radiant exposure for the center of the coupons weathered by participant 5 (Xe lamp, with the chamber controlled at 60°C and 50%RH).

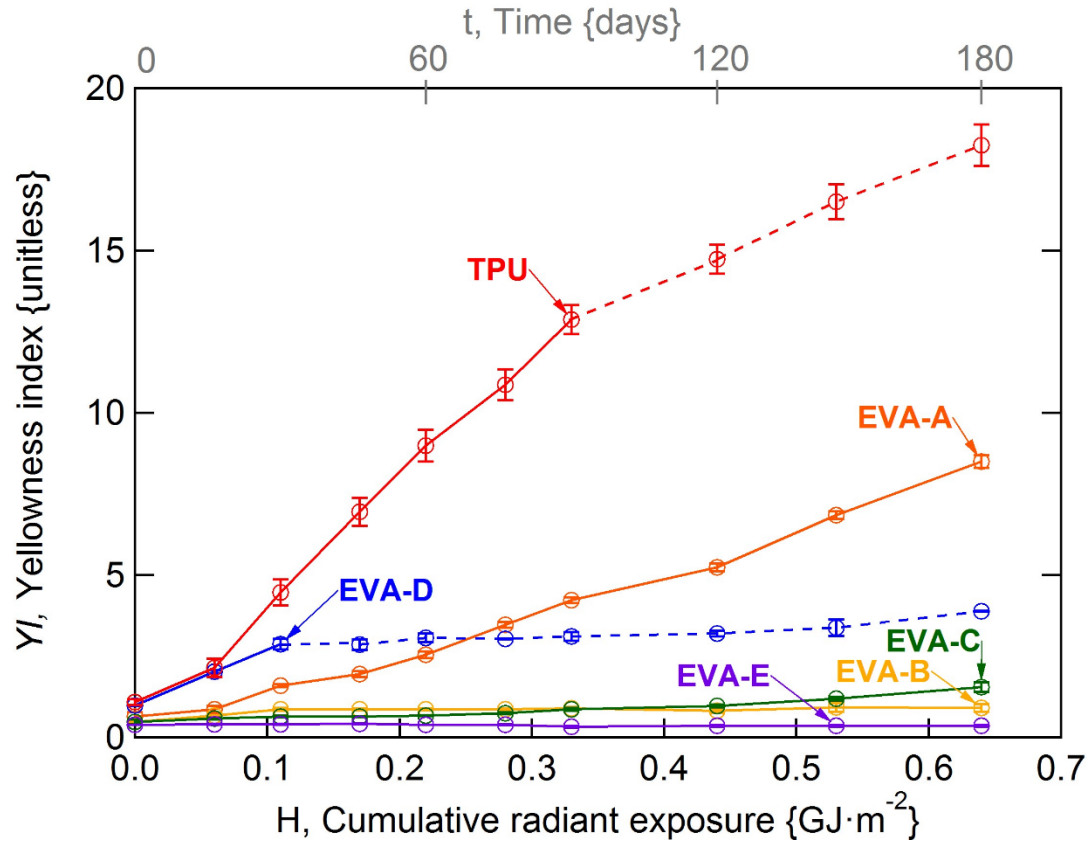

Figure 4: Change in YI with H for the center of the coupons weathered by participant 5 (Xe lamp, with the chamber controlled at 60°C and 50%RH).

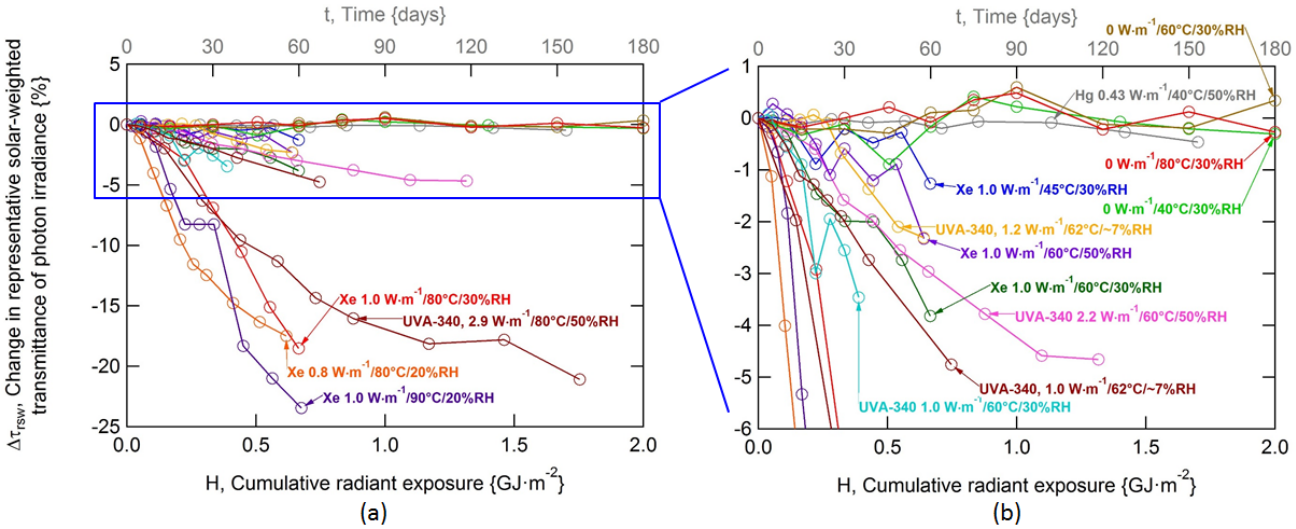

Figure 5: Overlay of the optical transmittance results for EVA-A, a known bad material, including: (a) all experiments in the study, and (b) the experiments showing less change in transmittance. Figure 3, Figure 14, and Figure 15 give a sense of the variation of transmittance measurements for the experiments in this study.

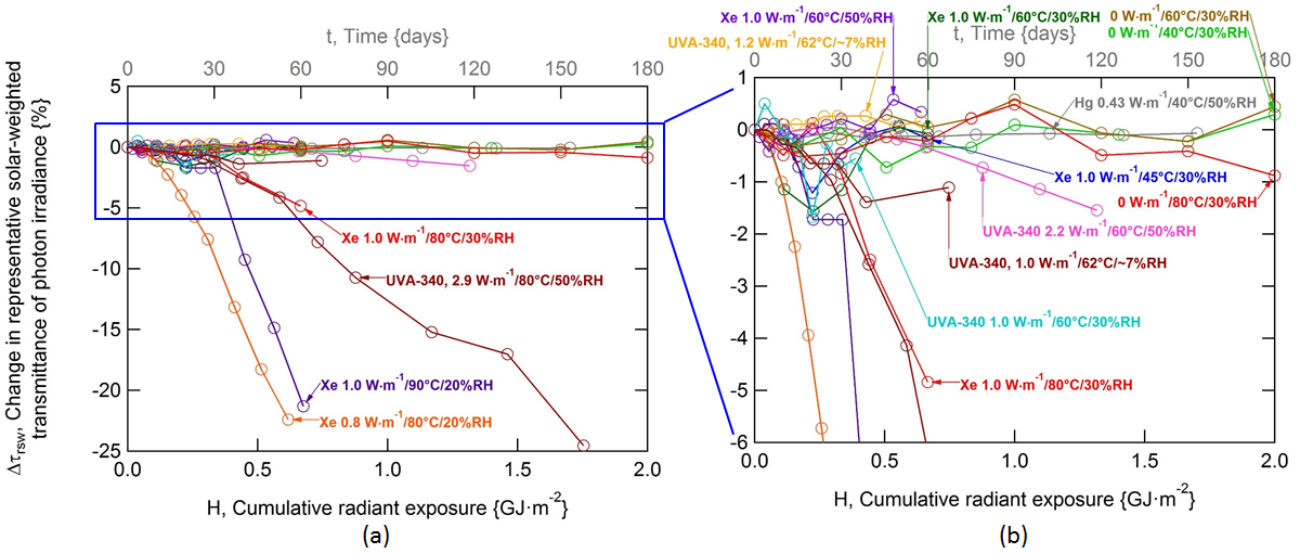

Figure 6: Overlay of the optical transmittance results for EVA-B including: (a) all experiments in the study, and (b) the experiments showing less change in transmittance. Figure 3, Figure 14, and Figure 15 give a sense of the variation of transmittance measurements for the experiments in this study.

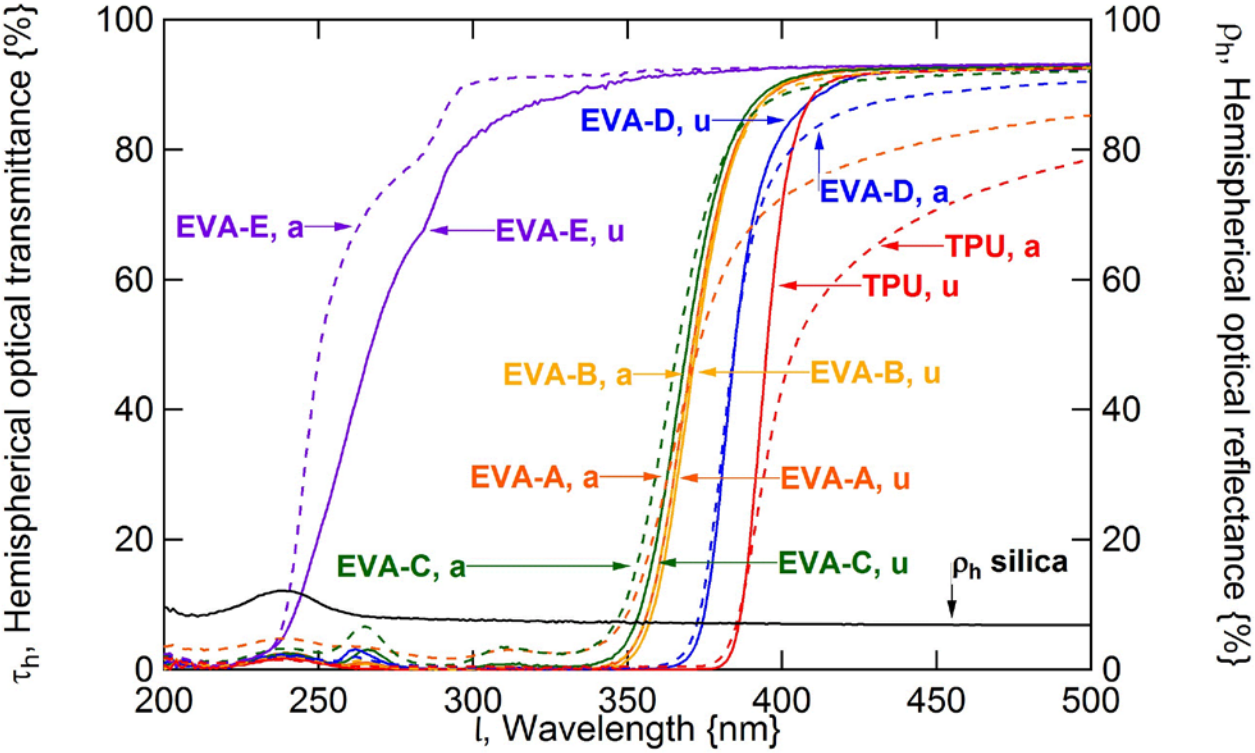

Figure 7: The UV spectral transmittance of the encapsulation materials examined. The suffix –u (solid lines) indicates the data for unaged specimens, whereas the suffix –a (dashed lines) indicates the final data for specimens weathered by participant 5 (Xe lamp, with the chamber controlled at 60°C and 50%RH).

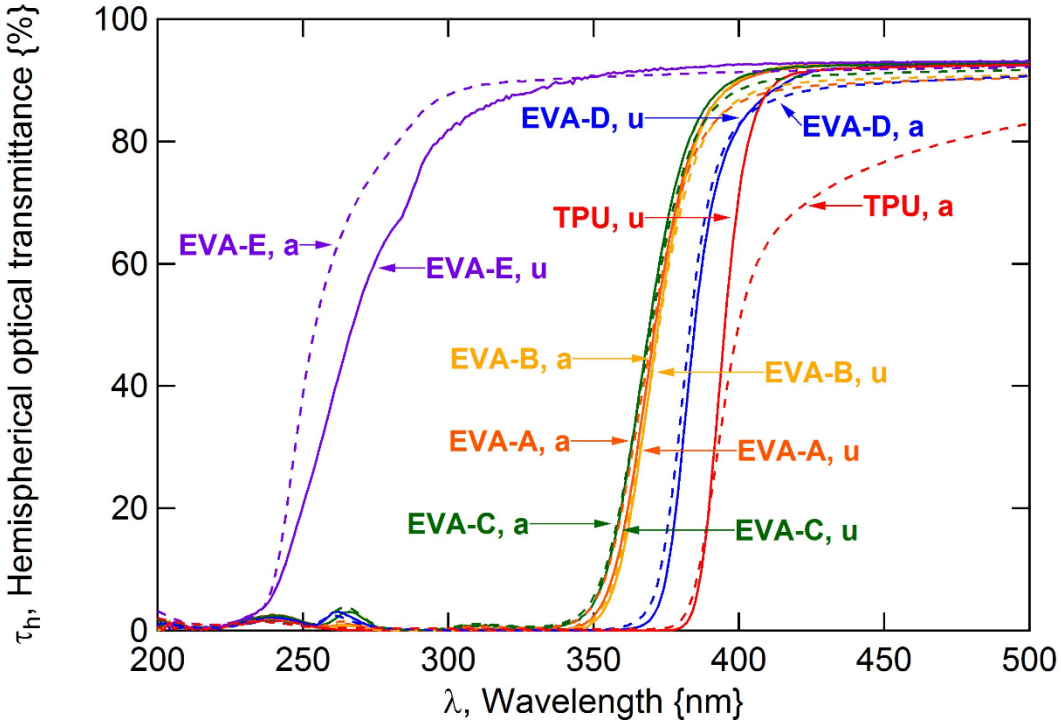

Figure 8: The UV spectral transmittance of the encapsulation materials examined. The suffix –u (solid lines) indicates the data for unaged specimens, whereas the suffix –a (dashed lines) indicates the final data for specimens aged by participant 6 (UVA-340 lamp, with the chamber controlled at 62°C and ~7%RH).

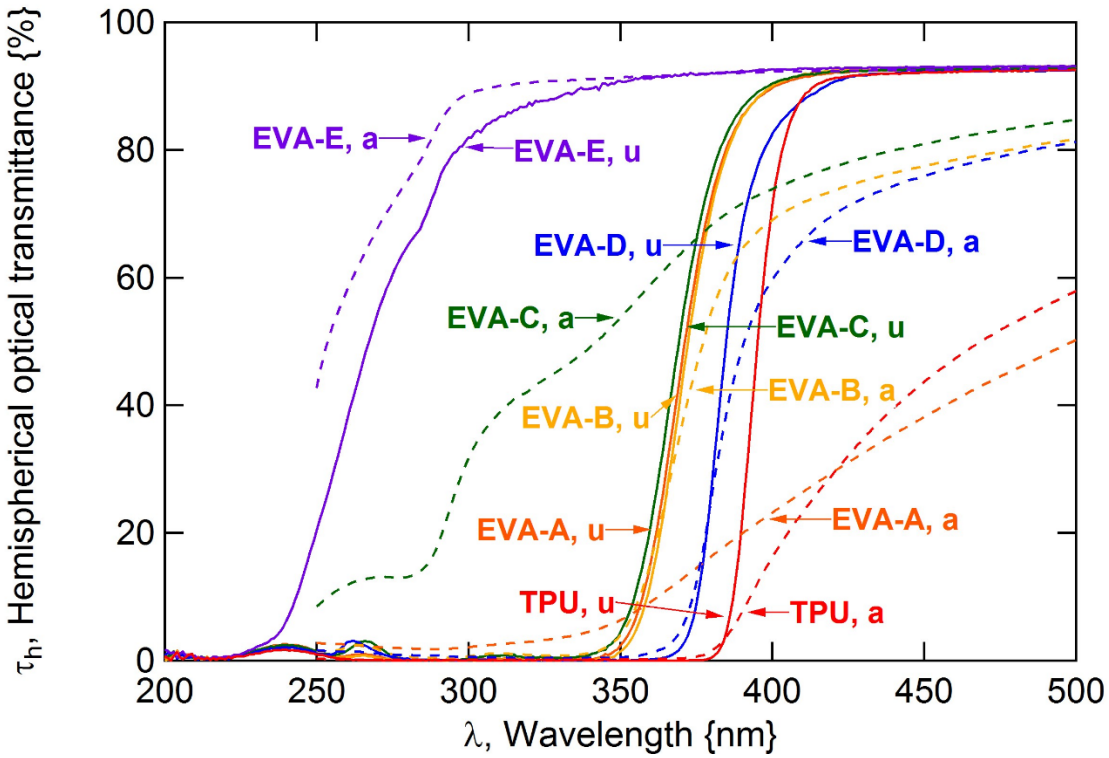

Figure 9: The UV spectral transmittance of the encapsulation materials. The suffix –u (solid lines) indicates the data for unaged specimens, whereas the suffix –a (dashed lines) indicates the final data for specimens aged by participant 1 (Xe lamp, with the chamber controlled at 80°C and 30%RH).

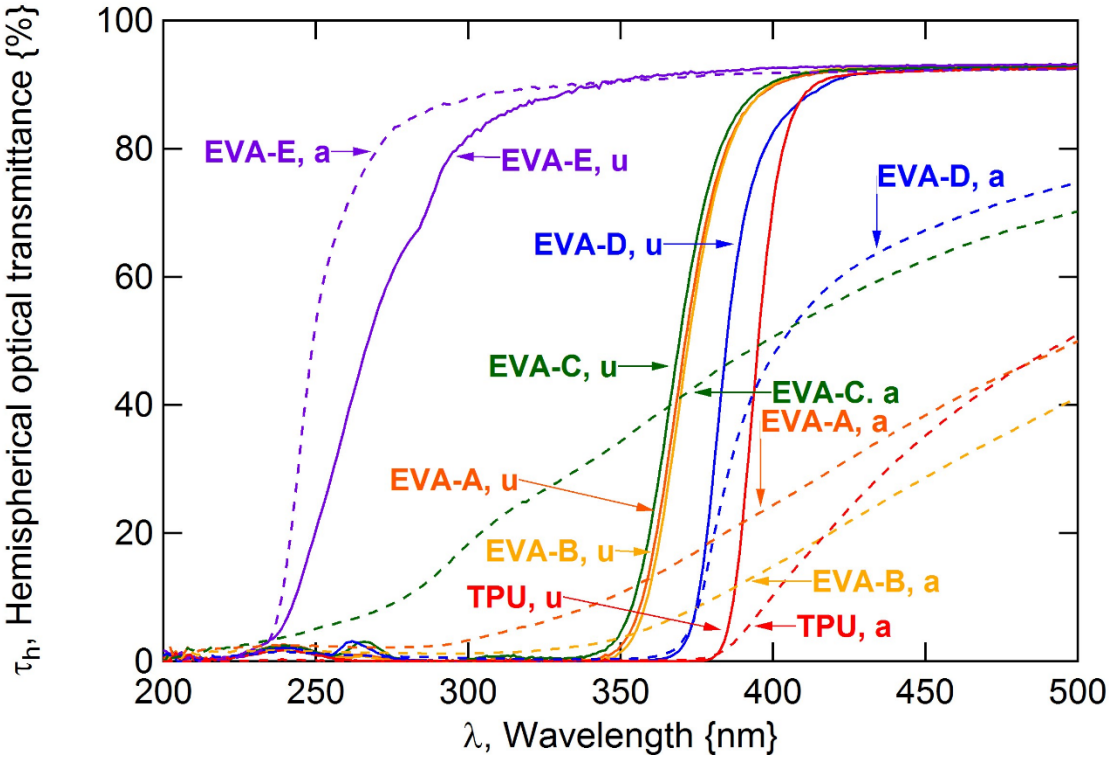

Figure 10: The UV spectral transmittance of the encapsulation materials. The suffix –u (solid lines) indicates the data for unaged specimens, whereas the suffix –a (dashed lines) indicates the final data for specimens aged by participant 2 (Xe lamp, with the chamber controlled at 80°C and 20%RH).

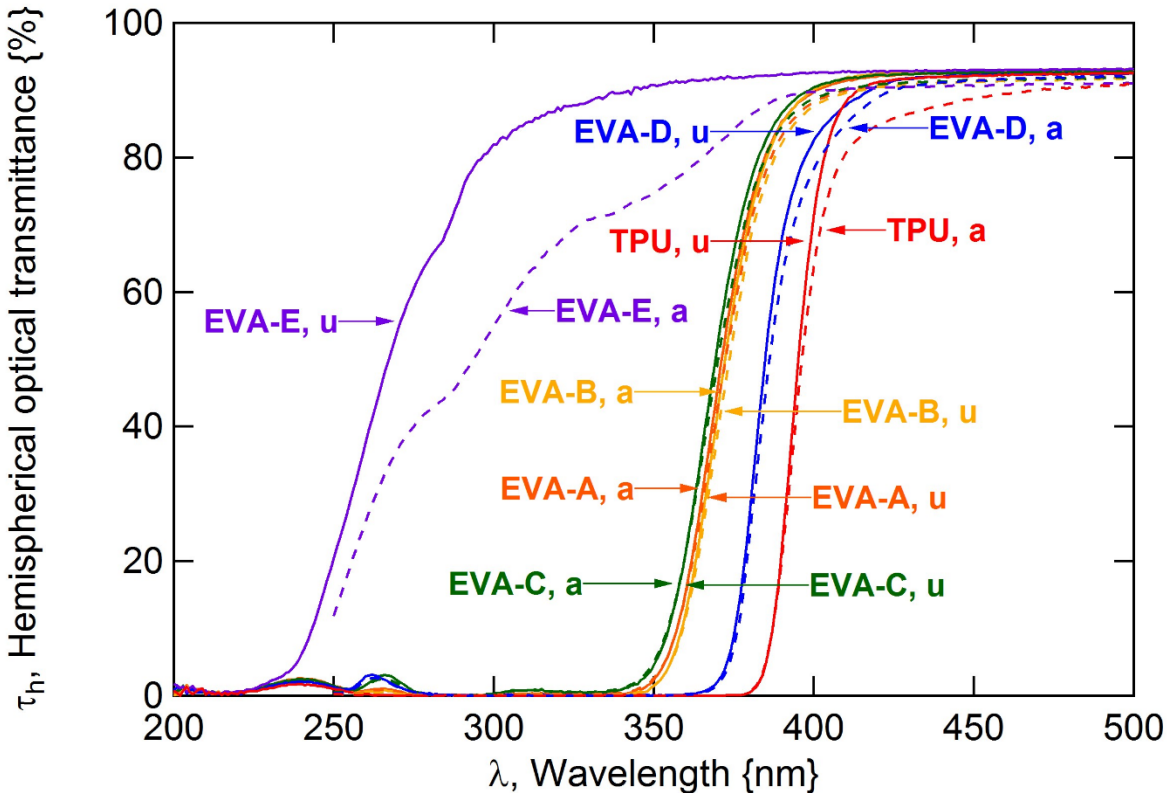

Figure 11: The UV spectral transmittance of the encapsulation materials. The suffix –u (solid lines) indicates the data for unaged specimens, whereas the suffix –a (dashed lines) indicates the final data for specimens aged by participant 4 (no irradiance, with the chamber controlled at 80°C and 30%RH).

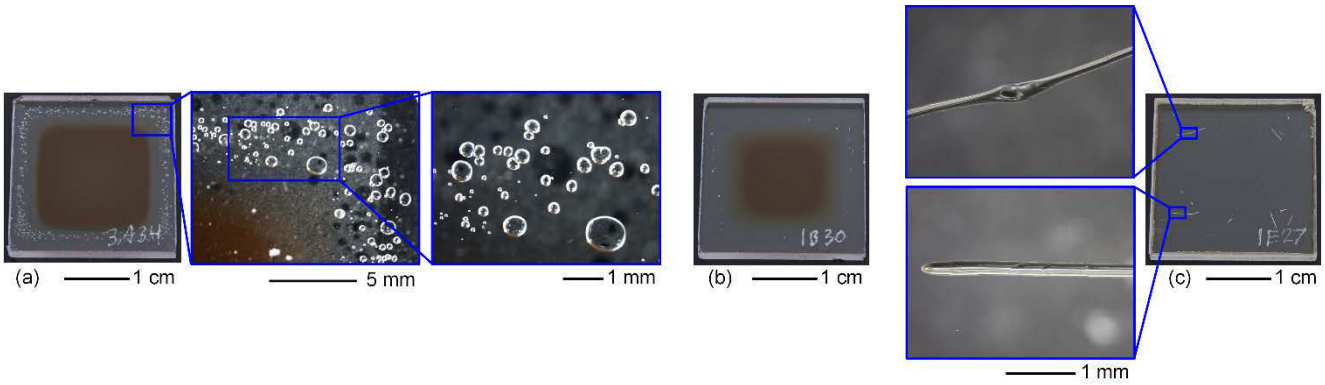

Figure 12: Visual appearance of some of the specimens from the hottest experiments in Figure 5(a), including: (a) round voids at the periphery of an EVA-A coupon for participant 2 [Xe lamp, with the chamber controlled at 80°C and 20%RH]; (b) round voids and heterogeneous discoloration in EVA-B for participant 2 [Xe lamp, with the chamber controlled at 80°C and 20%RH]; and (c) linear voids in EVA-E for participant 1 [~UVA-340 lamp, with the chamber controlled at 80°C and 50%RH]. The detail of some of the features is shown in insets to (a) and (c).

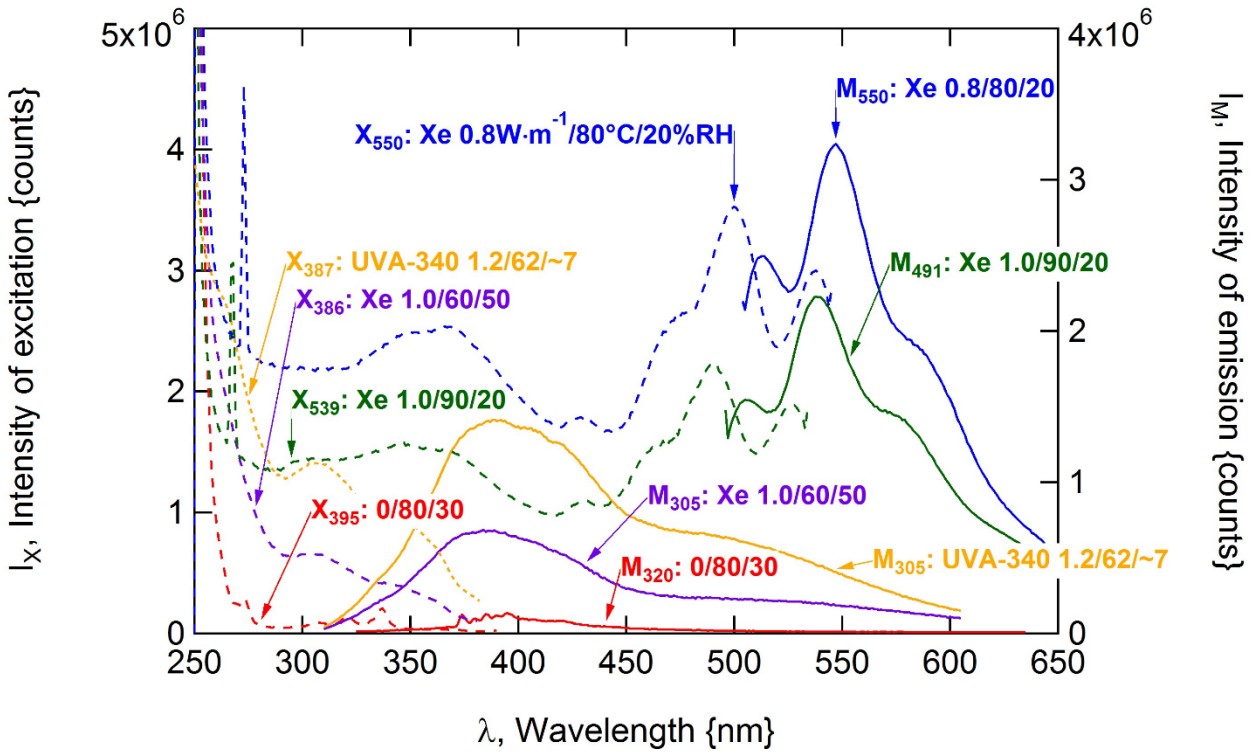

Figure 13: Comparison of fluorescence spectra for EVA-C. Excitation spectra (X, dashed lines on the left) and corresponding emission spectra (M, solid lines on the right) are shown for representative experiments. The nomenclature in the figure identifies the wavelength of greatest emission (for M) or wavelength monitored during excitation (X) as well as the source type, chamber temperature, and chamber relative humidity.

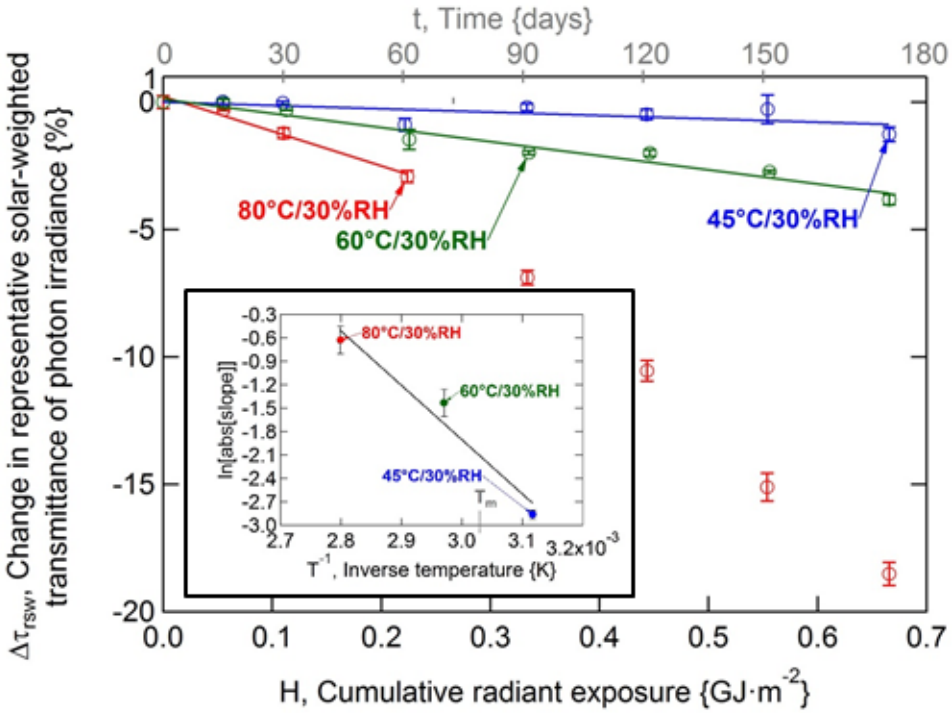

Figure 14: Comparison of change in transmittance with applied temperature for EVA-A. The same default irradiance and %RH conditions were used in separate Xe chambers, set at 45°, 60°, or 80°C. The slope from linear trend-line fits (through the origin, prior to an inflection in the data profile) was examined using an Arrhenius analysis, summarized in the inset.

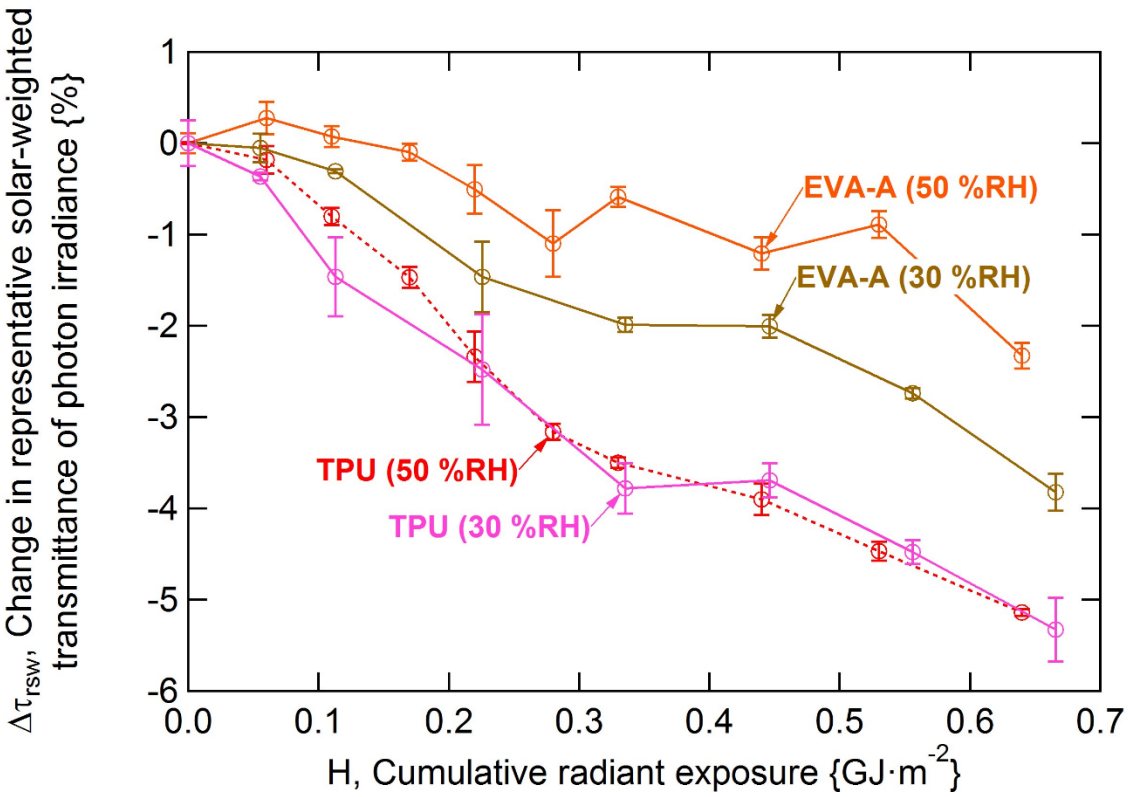

Figure 15: Comparison of change in transmittance for EVA-A and TPU with chamber relative humidity (30 %RH or 50 %RH). The default E_{340} of 1.0 W·m^{-2}·nm^{-1} and ChT of 60°C was applied in each Xe chamber.

Tables:

Table I: Summary of the test conditions applied in the present industry design type qualification and safety standards.

STANDARD (year)	TEST (index)	IRRADIANCE SOURCE	UV FILTER	E_b, BROADBAND IRRADIANCE {W·m^{-2}}	UV UNIFORMITY TOLERANCE (waveband range {nm})	IRRADIANCE SPECTRAL DISTRIBUTION (waveband range {nm})	H, CUMULATIVE RADIANT EXPOSURE {MJ·m^{-2}}	SPECIMEN TEMPERATURE {°C}	SPECIMEN RELATIVE HUMIDITY {%}
IEC 61215-2 (2016)	UV Preconditioning (MQT 10)	unspecified, λ≥280 nm	unspecified	≤250	≤±15% (280-320, 320-400)	3%≤H<10% (280-320)	54	60±5	unspecified
IEC 61730-2 (2016)	UV test (MST 54, nominal dose)	unspecified, λ≥280 nm	unspecified	≤250	≤±15% (280-320, 320-400)	3%≤H<10% (280-320)	54	60±5	unspecified
IEC 61730-2 (2016)	UV test (MST 54, increased dose)	unspecified, λ≥280 nm	unspecified	≤250	≤±15% (280-320, 320-400)	3%≤H<10% (280-320)	216	60±5	unspecified

Table II: Summary of the encapsulant materials examined in the study. Formulation additives are identified where they are known.

INGREDIENT	DESCRIPTION	MAKER	MASS {g}					
Elvax PV1400	EVA resin, 33 wt% VAc	E. I. du Pont	100	100	100	100	100	N/A
butylated hydroxytoluene	anti-oxidant (AO), heat stabilizer in EVA resin.	N/A	0.06	0.06	0.06	0.06	0.06	?
Z6030	siloxane primer, gamma-methacryloxy propyl trimethoxysilane	Dow-Corning Corp.	0.25	0.25	0.25	0.25	0.25	?
TBEC	curing agent, OO-Tertbutyl-O-(2-ethyl-hexyl)-peroxycarbonate	Arkema Inc.	N/A	1.5	1.5	1.5	1.5	?
Lupersol 101	curing agent, 2,5-Bis(tert-butylperoxy)-2,5-dimethylhexane	Arkema Inc.	1.5	N/A	N/A	N/A	N/A	?
Tinuvin 329	UV absorber, benzotriazole type	BASF Corp.	N/A	N/A	N/A	0.3	N/A	?
Cyasorb UV-531	UV absorber, benzophenone type	Cytec Industries Inc.	0.3	0.3	0.3	N/A	N/A	?
Tinuvin 770	hindered amine light stabilizer (HALS)	BASF Corp.	0.1	0.1	0.1	N/A	N/A	?
Tinuvin 123	non-basic aminoether-hindered amine light stabilizer (NOR-HALS)	BASF Corp.	N/A	N/A	N/A	0.1	0.1	?
Naugard P	AO, phenolic phosphonite	Chemtura Corp.	0.2	0.2	N/A	N/A	N/A	?
		Designation (Note)	EVA-A (known bad, "slow cure")	EVA-B (improved, "fast cure")	EVA-C (known good)	EVA-D (modern)	EVA-E (no UV absorber)	TPU (known bad)

Table III: Summary of the applied artificial weathering conditions as well as the optical characterization equipment used in the experiments.

	ARTIFICIAL WEATHERING					OPTICAL CHARACTERIZATION		
PARTICIPANT	IRRADIANCE SOURCE	IRRADIANCE FILTER (inner/outer)	E_{340}, IRRADIANCE AT 340 nm $\{W \cdot m^{-2} \cdot nm^{-1}\}$	ChT, CHAMBER TEMPERATURE {℃}	ChRH, CHAMBER RELATIVE HUMIDITY {%}	MAKE SPECTROPHOTOMETER	MODEL SPECTROPHOTOMETER	MEASUREMENT RANGE {nm}
1	Xe	D7869 compliant	1.0	45	30	Perkin Elmer	Lambda 1050	250-2500
1	Xe	D7869 compliant	1.0	60	30	Perkin Elmer	Lambda 1050	250-2500
1	Xe	D7869 compliant	1.0	80	30	Perkin Elmer	Lambda 1050	250-2500
2	Xe	s-boro/quartz	0.80	80	20	Perkin Elmer	Lambda 950	200-2500
3	HQI metal-halide	N/A	0.43	40	50	(a) Bruker & (b) custom	(a) Vertex 70 & (b) custom	320-2400
3	~UVA-340	N/A	2.17	60	50	(a) Bruker & (b) custom	(a) Vertex 70 & (b) custom	320-2400
3	~UVA-340	N/A	2.92	80	50	(a) Bruker & (b) custom	(a) Vertex 70 & (b) custom	320-2400
4	N/A	N/A	0	40	30	Perkin Elmer	Lambda 900	250-2500
4	N/A	N/A	0	60	30	Perkin Elmer	Lambda 900	250-2500
4	N/A	N/A	0	80	30	Perkin Elmer	Lambda 900	250-2500
5	Xe	D7869 compliant	1.0	60	50	Agilent	Cary 5000	200-2650
5	Xe	D7869 compliant	1.0	90	20	Perkin Elmer	Lambda 1050	200-2500
5	UVA-340	N/A	1.2	62	~7	Agilent	Cary 5000	200-2650
6	UVA-340	N/A	1.0	62	~7	Shimadzu	UV 2600	200-800
7	Xe	Daylight/quartz	1.0	60	30	Otsuka Electronics	MCPD-7700	250-800
7	UVA-340	N/A	1.0	60	~7	Otsuka Electronics	MCPD-7700	250-800

Table IV: Measured phase transition temperatures for the materials in this study.

MATERIAL	$T_g=T_\alpha$ {°C}	T_c {°C}	T_m {°C}
EVA-A	-32	37	57
EVA-B	-32	36	56
EVA-C	-32	37	56
EVA-D	-32	37	57
EVA-E	-33	37	57
TPU	-31	58	165
AVG[EVA]	**-32**	**37**	**56**

Table V: Summary of the Arrhenius analysis for the six materials in the study. As in Figure 14, the same default irradiance and %RH conditions were used in separate Xe chambers, where ChT was set at 45°, 60°, or 80°C.

	τ_{rsw}		YI	
MATERIAL	c_1, FREQUENCY FACTOR $\{s^{-1}\}$	E_a $\{kJ\cdot mol^{-1}\}$	c_1, FREQUENCY FACTOR $\{s^{-1}\}$	E_a $\{kJ\cdot mol^{-1}\}$
EVA-A	1.8E+08	58±8	3.5E+09	49±5
EVA-B	2.7E+06	50±8	2.9E+10	59±9
EVA-C	8.4E+03	36±8	1.7E+06	32±8
EVA-D	2.8E+06	47±8	1.9E+09	50±8
EVA-E	N/A	N/A	N/A	N/A
TPU	8.3E+07	53±8	7.9E+09	50±4

Table VI: Summary of results of relative degradation analysis. The degradation factor (ratio of the slope for the experiment at 50%RH to the slope for the experiment at 30%RH in Figure 15) is given for the parameters of transmittance and yellowness index.

	τ_{rsw}	YI
MATERIAL	k_H (for τ_{rsw}) {unitless}	k_H (for YI) {unitless}
EVA-A	0.4±0.2	1.0±0.1
EVA-B	N/A	N/A
EVA-C	N/A	0.9±0.1
EVA-D	N/A	0.4±0.0
EVA-E	N/A	N/A
TPU	1.1±0.1	1.2±0.1